Geomechanical Study – Small Gas Fields in the Netherlands

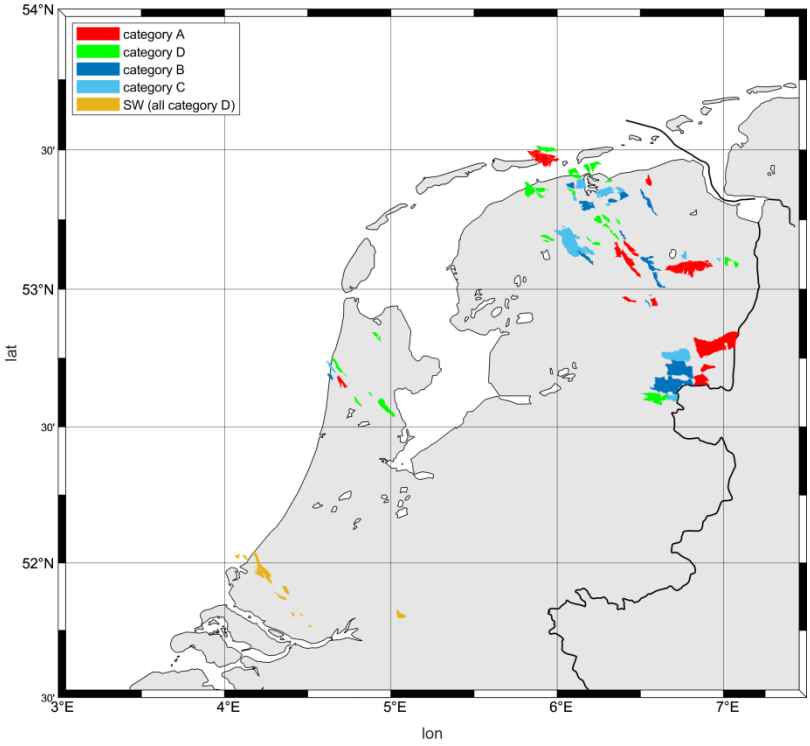

SODM002

Report title:	Geomechanical Study – Small Gas Fields in the Netherlands
Author(s):	Robert Vörös, Stefan Baisch
Report date:	5.12.2018
Prepared for:	State Supervision of Mines (SodM)
Version:	Version 1
Archive No.:	SODM002

Contents

Contents

1 BACKGROUND & SCOPE

In The Netherlands gas has been produced from approximately 166 onshore gas fields. Since the mid-1980s, approximately 1,400 induced earthquakes were recorded in the vicinity of producing gas fields. Most earthquakes were associated with the largest of those gas fields in Groningen. Some of the smaller gas fields, however, also produced significant seismicity giving rise to seismic hazard concerns.

For operators and the regulator it is of primary importance to understand the circumstances under which induced seismicity occurs. This is a strict requirement for seismic hazard assessments.

In previous studies (e.g. van Eijs et al., 2006; van Thiener-Visser et al., 2012; van Wees et al., 2014; Fekkes, 2016) geological and operational parameter were correlated with induced seismicity observations. As a result, key parameters associated with induced seismicity have been identified forming the basis for subsequent seismic hazard assessments. Conceptually, it is reasonable to assume that the key parameters used for seismic hazard assessment are indeed related to the occurrence of induced seismicity. A physics-based geomechanical analysis of the induced seismicity, however, has not been conducted for most of the small gas fields.

Compared to the evidenced-based approach applied currently (van Thiener-Visser et al., 2012), a physics-based approach has the potential to assess seismic hazard also in a scenario which is outside the range of previous experience. A limiting factor, however, is the uncertainty associated with subsurface conditions.

The focus of the current study is on developing a framework for numerically simulating poro-elastic stresses in producing (small) onshore gas fields in The Netherlands. This requires a compilation of available information on subsurface parameters, as well as a numerical modelling workflow that allows for running a large number of different models for investigating sensitivities to unconstrained parameters. These simulations shall address the guiding question why seismicity has occurred in certain gas fields, whereas other gas fields remained seismically quiet.

A key aspect of this work is to investigate whether the relevant geomechanical processes leading to seismicity can be reproduced by (simple) numerical models based on the known reservoir parameters. If that is the case, the method developed in this study could constitute an essential component for future seismic hazard assessments.

2 SUMMARY

The study is organized in two parts. In the first part, a comprehensive data base of subsurface and operational parameters is compiled for small onshore gas fields in the Netherlands. The data base is mainly built from existing data and reflects the current knowledge of subsurface conditions in the gas reservoirs. It contains information on the reservoir geometries, lithology, mapped faults and rock mechanical parameters, as well as reservoir pressure, pressure depletion and induced seismicity. The main database comprises 81 onshore reservoirs, 27 of which were previously associated with seismic activity related to gas production. Accounting for the location uncertainty of the earthquakes, reservoirs were additionally categorized in 'most likely' associated with induced seismicity (category A), 'possibly associated' (categories B, C) and 'most likely not associated' with seismicity. The data base has been exported to EXCEL and is attached to this study.

In the second part, an automatized workflow is developed for numerically simulating poro-elastic stresses associated with gas production. Scripting is used to setup 2D numerical models for geomechanical simulations. The key components in this scheme are the reservoir specific parameters in the database and an additional set of parameters that are not generally available and subject to larger uncertainties. These two types of parameters are referred to as 'constrained' and 'unconstrained' parameters, respectively, and constitute the parameter input required for the simulations.

The unconstrained parameters are treated as free variables that are used for matching the observed seismicity. If chosen individually for each reservoir, the unconstrained parameters offer a sufficient degree of freedom for perfectly matching the observed occurrence and non-occurrence of seismicity. This matching strategy, however, has no forecasting capabilities. Following Occam's razor, the number of free model parameters is therefore kept at a minimum.

In a calibration procedure, an optimized set of unconstrained parameters is identified, yielding the best agreement between simulated stress criticality and observed seismicity ('match'). Initially, unconstrained parameters were assumed globally, i.e. the same set of unconstrained parameters is assumed for all reservoirs. As a requirement in the calibration procedure, only those parameter combinations were considered which yield overcritical stress conditions for all category A ('most likely associated with seismicity') reservoirs. By this requirement, numerical simulations tend to be conservative in the sense that all reservoirs which were actually associated with induced seismicity are also 'simulated' to respond seismically. Mismatch between simulations and observations are restricted to gas fields which are not associated with induced seismicity ('over prediction').

The calibration procedure resulted in different combinations of unconstrained parameters all providing a 100% match of the 12 category A reservoirs. The simultaneous match of category D reservoirs ('most likely not associated with seismicity'), however, did not exceed 30%. Systematic mismatches were observed in the South-West of The Netherlands where numerical simulations frequently yield overcritical stress conditions, although none of the gas fields is associated with seismicity. By introducing a different stress-ratio for the South-West

of The Netherlands, motivated by the regional distribution of salt overlying the reservoirs, the match of category D reservoirs was increased to approximately 50%. The associated combination of unconstrained parameters is documented in section 4.4.3 and is referred to as model BFM-SW.

Based on the BFM-SW model, a consistency test was successfully applied to category B, C reservoirs ('possibly associated with induced seismicity'). For each earthquake attributed to gas production in The Netherlands, it was confirmed that overcritical stress conditions were simulated in at least one gas reservoir within 2.5 km distance to the epicentre, which is considered to be the epicentre location uncertainty.

Although different combinations of unconstrained parameters produce an equal number of observation matches, the same set of reservoirs tends to be matched by different best-fitting parameter combinations. This indicates that the constrained reservoir parameters truly carry information about whether or not a gas field responds seismically to gas production. Despite making global assumptions regarding the unconstrained parameters, this information can at least partly be extracted by the proposed workflow. This is an encouraging result.

It is acknowledged, however, that the proposed workflow results in a significant over prediction. The ~50% mismatch of category D reservoirs could result from parameter uncertainty or from oversimplifications in the geomechanical model. We consider the parameter uncertainty to be the relevant factor. In particular, the approach of making global assumptions for parameters that are typically not known tends to oversimplify. Future research could focus on assessing additional reservoir parameters such as fault dip and throw, which are currently handled by global assumptions.

The BFM-SW model was also used to study the future stress evolution in each gas field until the end of production. Simulation results indicate that further category D gas fields might produce seismicity towards the end of their lifetime. Only 10 category D gas fields remain at sub-critical stress conditions at the end of production.

Simulation results from this study are compared to the DHAIS estimates of earthquake occurrence probability, which are based on an empirical approach (van Thienen-Visser, 2012). The DHAIS values also exhibit a considerable number of mismatches in the sense that either a seismically active reservoir of category A was assigned a low probability for earthquakes or a category D reservoir was assigned a high probability. The DHAIS mismatches, however, seem to be uncorrelated with the mismatches obtained with the physics-based approach.

3 DATABASE

Information on gas fields in the Netherlands is publicly available from various data sources (Figure 1). The basis for the current study is a comprehensive data compilation by van Thienen-Visser et al. (2016), which had to be extended in this study. The underlying primary data sources are nlog.nl (e.g. providing *Winningsplan*) and dinoloket.nl, containing information on subsurface formation and rock type. A detailed list of the data sources used for this study is provided in Appendix A.1. Based on these data sources, a database (referred to as the 'main database') was set-up, containing information on small, onshore gas fields in The Netherlands.

The main database contains reservoir specific parameters that are relevant for the numerical simulation of depletion related stresses on reservoir faults. An overview of the most relevant database entries is provided in Table 1. These are primarily geometrical parameters of the reservoir layer and crosscutting faults, rock mechanical parameters of the reservoir layer and the over-/underburden as well as hydraulic parameter, i.e. reservoir pressure and depletion level. In addition, the main database contains information on seismicity associated with individual reservoirs. The main database covers only those reservoir specific parameters, which are constrained by observation data ('constrained parameters'). Those parameters which are typically unconstrained by observation data ('unconstrained parameters') enter as variables into the numerical simulation procedure in chapter 4. These include parameters with regional character, such as the undisturbed (virgin) stress field, but also parameters which are specific to a reservoir, e.g. the throw of reservoir faults.

The main database is built from various data sources. In the following sections, selection criteria, ranking of data sources and the rules for dealing with ambiguous or missing information are defined.

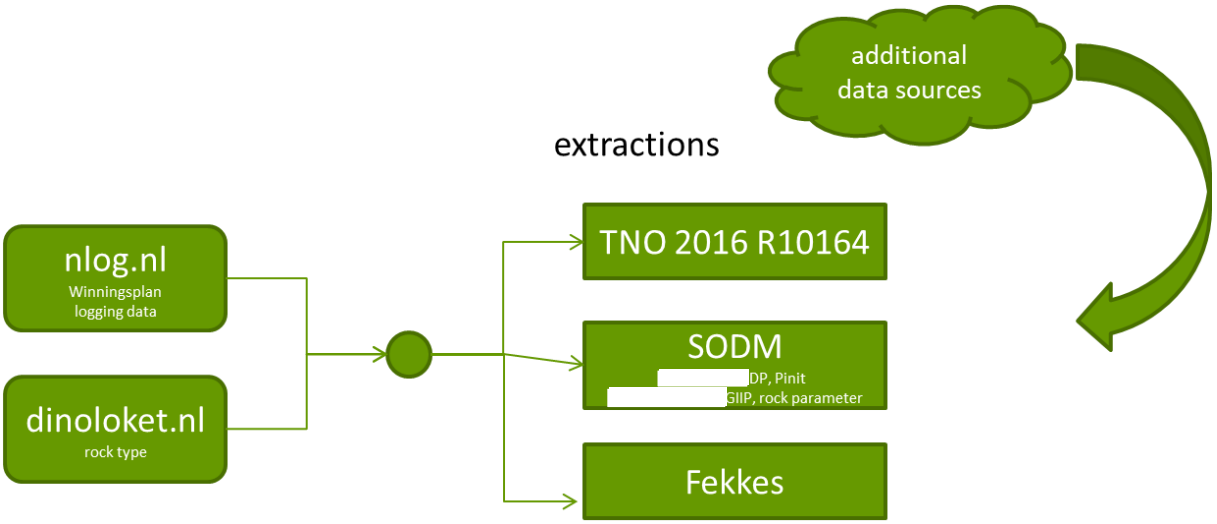

Figure 1: Overview of most relevant primary data sources and data compilations. Most extractions are based on the primary data sources. In some cases, additional (confidential) data was provided by the operators to SODM. Associated data was made available for the current study.

parameter type	parameter
ID	reservoir name (+ additional suffix for respective formation in case of multiple reservoir fields)
geometry	reservoir depth
	reservoir thickness
	thickness overburden / underburden layer
hydraulic (reservoir)	initial pressure
	depletion level • at onset of seismicity (seismically active) • current / leaving (seismically not active)
rock (reservoir, over-/underburden)	Young's modulus (range) Poisson's ratio (range)
fault orientation / type	strike (discretized) / boundary (hanging wall,foot wall), internal

Table 1: Overview on the most relevant, reservoir specific parameter in the database.

3.1 Field selection

All onshore gas fields listed in van Thienen-Visser et al. (2016) are considered in the current study. In addition, onshore gas fields that have shown seismic activity but which are not covered by van Thienen-Visser et al. (2016) have been integrated into the main database (see Table 2).

In several fields, gas is produced from different formations. These include Den Velde DC (carboniferous) and ZE (Zechstein), Middelie ROSL (Slochteren) and ZE, Oosterhesselen DC and ZE. In the numerical simulations (chapter 4), these are referred to as ‘multiple reservoirs’ and each formation is treated as an individual model (‘reservoir’). With this definition, a total number of 81 reservoirs results.

no.	reservoir name
1	Bergermeer
2	Metslawier
3	Norg
4	Roden
5	Roswinkel
6	Slootdorp*

Table 2: List of seismically active reservoirs that have been added to the reservoirs covered by van Thienen-Visser et al. (2016). Note that Slootdorp has been re-classified as seismically not active following initial comments by SodM.

3.2 Reservoir depth

Reservoirs depth was taken from the respective *Winningsplan* or, if not available, from wellbore profiles in nlog.nl. Reservoir depth varies from 1,900 m to 4,000 m (Figure 2)

.

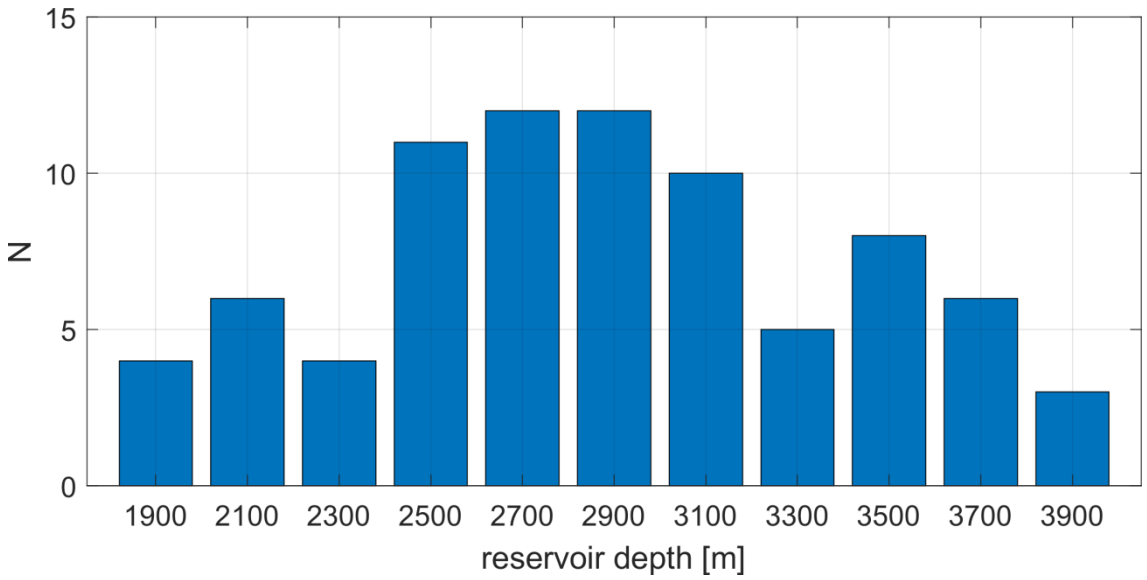

Figure 2: Histogram of reservoir depth. The parameter ranges from 1,900 m to 4,000 m for the reservoirs considered in this study.

3.3 Reservoir thickness

Reservoir layers as defined by van Thienen-Visser et al. (2016) are the basis for the determination of reservoir thickness. Reservoir thickness is usually stated in the *Winningsplan*, but inconsistencies were noted when comparing different *Winningsplan* for the same reservoir. Therefore, consistency checks were performed using wellbore profiles from nlog.nl (either single wells or averaged values from multiple wells). In case of non-existing or contradictory information in the *Winningsplan,* values derived from wellbore profiles were preferred. Reservoir thickness varies from 30 to 289 m (Figure 3).

Note:

The data base also includes the thickness of the over- and underburden layers, which was determined from wellbore profiles provided on nlog.nl. The thickness of the over- and underburden, however, was not implemented into the geomechanical models where these layers were extrapolated to the model boundaries.

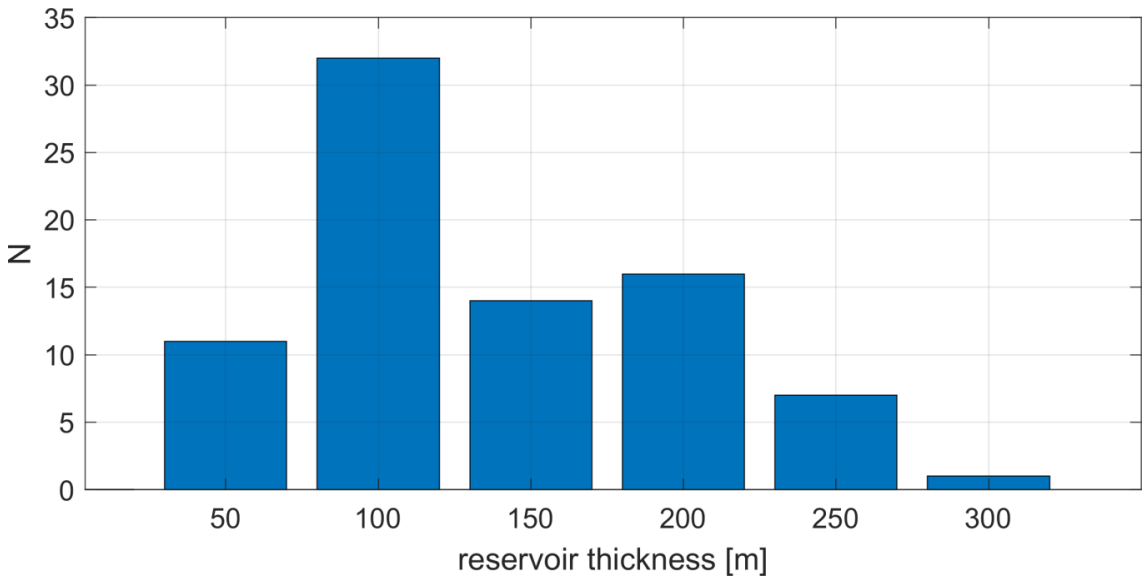

Figure 3: Histogram of reservoir layer thickness. The parameter ranges from 30 m to 289 m for the reservoirs considered in this study.

3.4 Reservoir rock type and elastic rock parameter

The reservoir rock type serves as a proxy for the elastic rock parameters required for the geomechanical simulations (i.e. Young's modulus and Poisson's ratio). If possible, rock type (e.g. sandstones, dolomites etc.) was adopted from van Thienen-Visser et al. (2016). If this information was not available, data was taken from dinoloket.nl, where the rock composition of a formation or the formation members are stated.

For assigning elastic rock parameters to rock type, the different rock types associated with reservoir, overburden and underburden have been grouped into superordinate classes

according to Table 10 in Appendix A.2. Comparing those classes with parameter values for individual reservoirs that have been provided by SodM (SodM 2018a), a parameter range for Young's modulus and Poisson's ratio was assigned to each rock type.

3.5 Fault parameter

Fault characteristics play a decisive role for the occurrence of induced seismicity. For the geomechanical simulations, the relevant parameters are fault strike, dip, throw and fault stability.

In the typical reservoir Winningsplan, a horizontal section of the reservoir is displayed with mapped faults at reservoir level. From these maps, fault strike and dip direction can be inferred (see example in Figure 4). Other fault parameters (dip, throw and fault stability) are usually not available and are considered unconstrained parameters.

As part of the current study, faults were grouped according to their orientation by visual inspection. A resolution of 30° was chosen (Figure 5). Although all mapped faults entered into the database, only faults extending over at least 1 km laterally ('large faults') were considered in the geomechanical simulations.

Further information is required to characterize faults with respect to the location either inside or at the boundary of the reservoir. The fault location has a direct impact on the geomechanical simulation results. For internal faults, a two sided depletion needs to be considered, whereas one-sided depletion applies to boundary faults. For boundary faults, it has to be additionally stated whether the reservoir is located in the footwall or in the hanging wall (compare Figure 6). This information can also be obtained from the maps provided in the *Winningsplan* (Figure 4).

In total, 374 different faults (> 1 km) are included in the main database. Figure 7 shows the associated distribution of the strike directions.

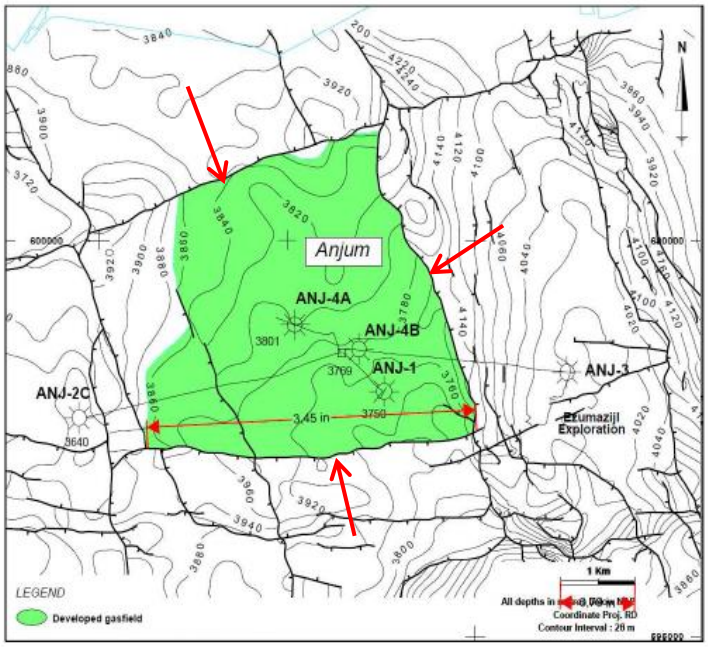

Figure 4: Example figure from a Winningsplan (Anjum) outlining the reservoir (green) and fault trajectories (red arrows).

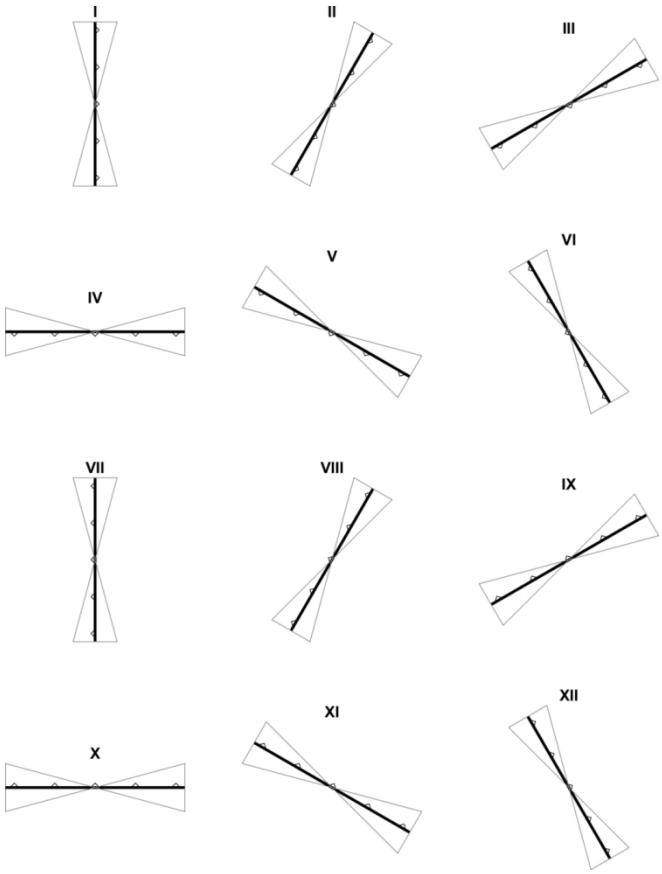

Figure 5: Classification scheme of fault classes according to strike direction (sampled every 30° → 0°, 30°, 60° …, 330°). Triangles denote dip direction of the fault class.

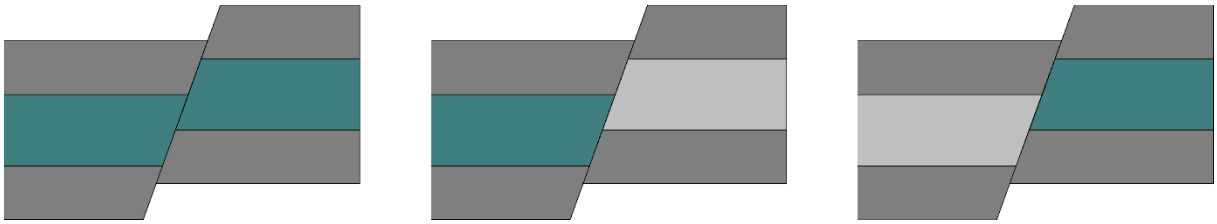

Figure 6: Fault types considered in this study: Internal fault (left) at which the reservoir layer (blue) is offset across the fault, boundary fault (center) with the reservoir located in the hanging wall and boundary fault (right) with the reservoir located in the foot wall.

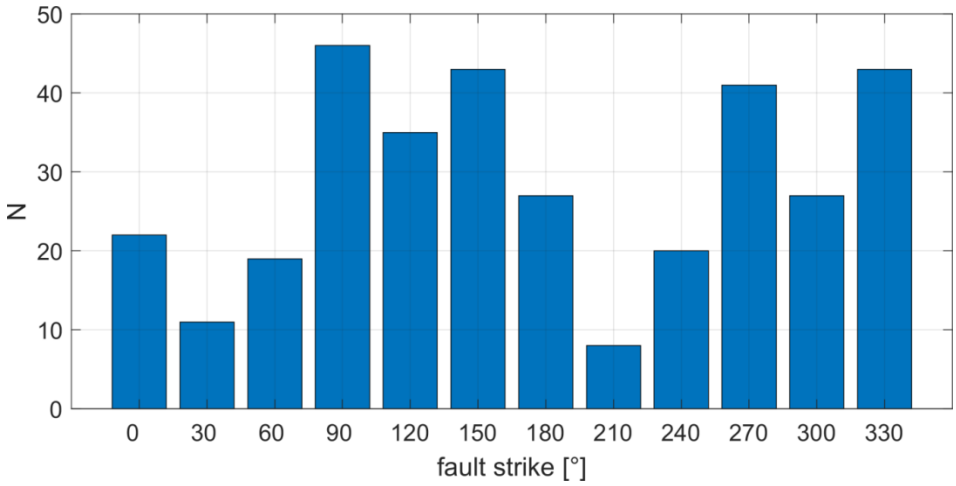

Figure 7: Histogram of strike direction for the reservoir faults > 1 km in the main database.

3.6 Reservoir pressure

The initial reservoir pressure (i.e., the pressure in the reservoir at production start) was adopted from the *Winningsplan*. If not mentioned in the *Winningsplan*, data from (2017) or Fekkes, (2016) was used. Data for the Norg reservoir was provided by SodM (2018b). Figure 8 gives an overview of the initial reservoir pressure.

The reservoir depletion level entering into the numerical simulations is either the current pressure level (as of 2017) for seismically non-active reservoirs or the pressure level at the time when the first earthquake occurred in a seismically active reservoir. With this definition, stress conditions simulated numerically (either super- or sub-critical) can directly be compared to observations (either seismically active or quiet). The primary data source for reservoir depletion is (2017) and SodM (2018a,b). Four reservoirs are not included in these data sources: Blija-Zuid, Brakel, Heinenoord and Wieringa. Depletion in these reservoirs was estimated utilizing GIIP (Gas Initially In Place)-values and the produced gas volume (see Appendix A.3), the latter of which is provided by the nlog.nl web-resource.

GIIP-data was provided by SodM (SodM 2018c). Depletion values range from -17 bar down to -513 bar (Figure 9).

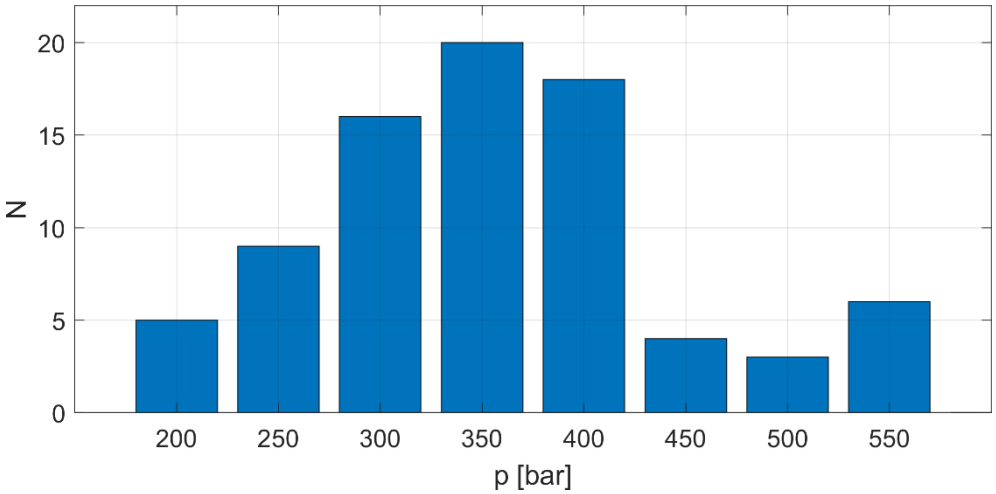

Figure 8: Histogram of initial reservoir pressure.

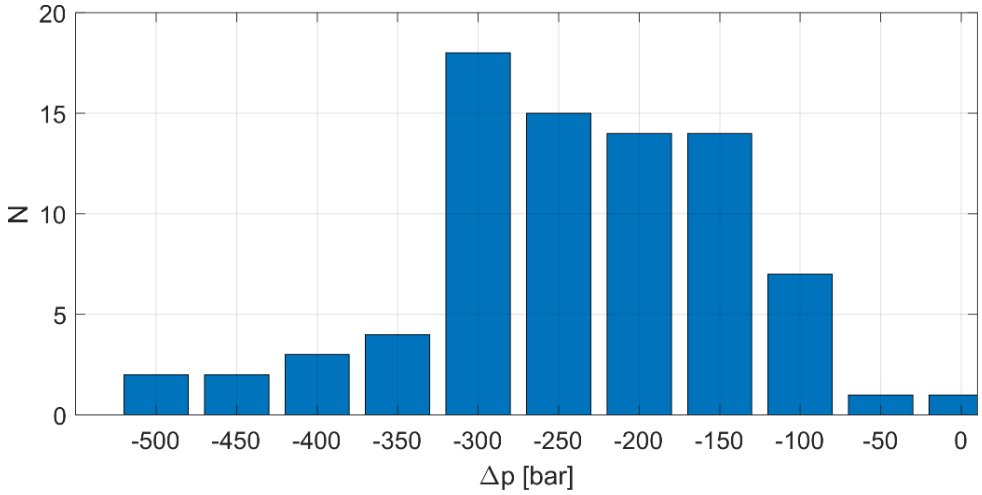

Figure 9: Histogram of reservoir depletion.

3.7 Seismicity associated with reservoirs

Based on the KNMI seismic catalogue as of January 2018 (http://www.knmi.nl), induced events were assigned to individual reservoirs. This assignment is based on temporal consistency with reservoir production and spatial proximity of the event epicentre and the reservoir. In total, 272 events in the magnitude range M_L=-0.8 to M_L=3.5 are associated with production from small gas fields. From the 81 reservoirs considered in this study, 27 are associated with seismic activity. The seismic event association in the main database is mostly consistent with van Thienen-Visser et al. (2016).

Figure 10 shows the number of seismic events associated with each reservoir. The largest number of events is associated with the reservoirs Annerveen, Eleveld, Roswinkel and Emmen (each more than 10 detected events), whereas the remaining reservoirs are associated with less than 10 events. Note, however, that the lower magnitude detection threshold varies significantly over The Netherlands.

Results of initial geomechanical simulations gave rise to the question, how certain the association of an earthquake to a specific gas field is. Associations are critically depending on the accuracy of earthquake epicentres, which is typically in the order of one to several kilometres. In case of neighbouring gas fields, a unique association of an earthquake to a specific gas field may not always be possible. To avoid bias from falsely associated earthquakes, an additional classification scheme is introduced (Figure 11).

Assuming an average lateral epicenter location uncertainty of 2.5 km for the whole of The Netherlands, those reservoirs were identified, which most likely produced (category A) and did not produce (category D) seismicity.

A category A reservoir is defined if at least one seismic event exists that can only be associated with this particular reservoir even when accounting for a lateral location uncertainty of 2.5 km. Similarly, category D reservoirs are those reservoirs, which cannot be associated with a single earthquake from the catalogue even when accounting for 2.5 km lateral location uncertainty.

The other two categories are defined by epicentres located within 2.5 km distance of at least two reservoirs (‘possibly’). These reservoirs are classified as category B if associated with earthquakes in the main database, or category C if not associated.

Exceptions have been introduced in case local seismic networks exist (Roswinkel) or reservoir production is not consistent with event times. In total, 12 category A reservoirs result, 39 category D reservoirs, 15 category B and 15 category C reservoirs. Categories B and C are equivalent in the context of the current study.

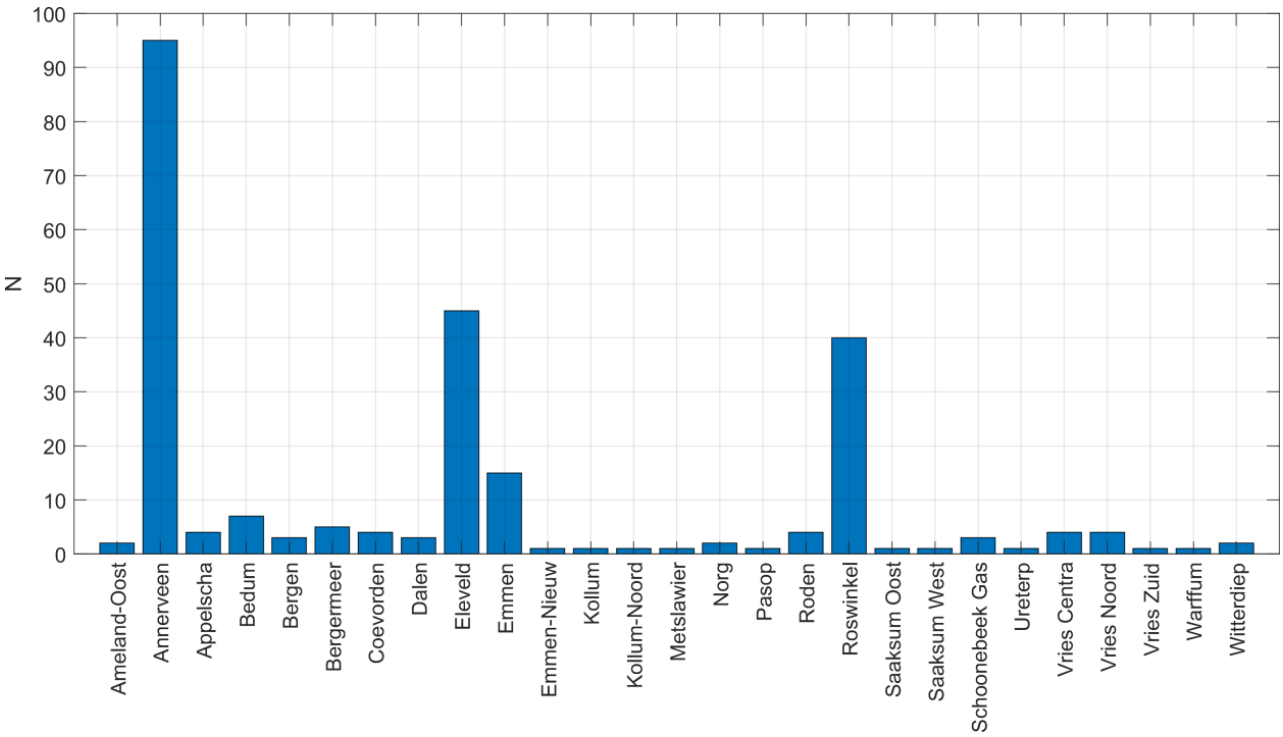

Figure 10: Number of seismic events associated with the 27 gas reservoirs classified as seismically active.

likely **associated in main database** **A**	**possibly** **associated in main database** **B**	**possibly** **not associated in main database** **C**	**likely not** **not associated in main database** **D**

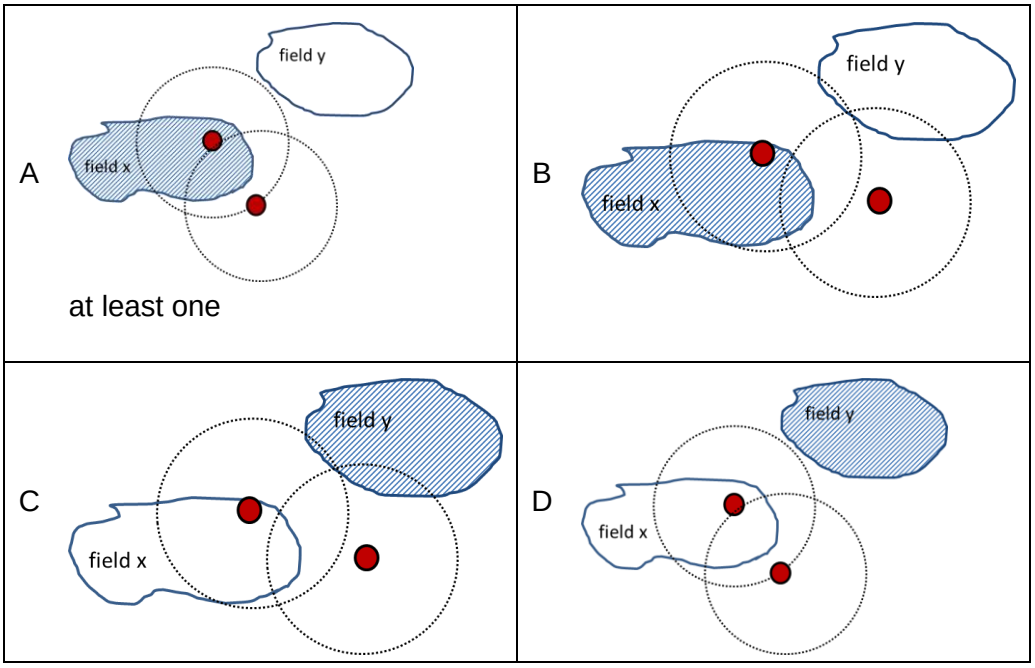

Figure 11: Schematic display of the classification scheme. See text for details.

4 GEOMECHANICAL SIMULATIONS

Geomechanical simulations are performed to determine the state of stress on reservoir faults prior and after reservoir depletion due to gas production. The input parameters for these simulations are the reservoir specific parameters ('constrained parameters') from the main database. The unconstrained parameters are treated as free variables that are used for matching the observed seismicity. The simulations are conducted utilizing a 2D finite element numerical reservoir model similar to the model used by van den Bogert (2016). The model is implemented in COMSOL Multiphysics in combination with the MATLAB scripting environment. The simulations conducted in the framework of this study are facilitated by an automated model setup to cope with the large number of numerical models investigated in this study. In total, approximately 10^6 numerical models were simulated in the course of this study.

4.1 Definition of fault criticality

Shear capacity utilization (SCU) is used to quantify the level of stress criticality. SCU is defined as (e.g von den Bogert, 2016)

$$SCU = \frac{\tau}{\mu(\sigma_n - p) + C_0}. \qquad \textit{Equation 1}$$

where τ, σ_n and p denote shear-, normal-stress and fluid pressure on the fault. The coefficient of friction μ and cohesion C_0 control the strength of the fault.

4.2 Model Setup

4.2.1 Model geometry

The model setup closely follows van den Bogert (2016), where stress variations on the faults related to reservoir depletion are simulated in a 2D-model centered on a fault (Figure 12). Homogeneous depletion within the entire reservoir layer is assumed. Although the 2D approach is a simplification, it is nevertheless considered to be suitable for studying first order effects.

The 2D geometry includes a reservoir layer and an over- and underburden layer. The layer stack is intersected and potentially offset by a dipping fault (Figure 13). The lateral and vertical model extensions are 2 km and 6 km, respectively. No normal displacement is allowed at the lateral and bottom model boundaries. The model boundary at the top is implemented as a free surface. Stress computations are conducted along the fault with a spatial sampling of 0.1 m in dip direction. Hence, a corresponding FEM-mesh is chosen with a higher resolution along the reservoir fault (Figure 13). Model setup and implementation have been benchmarked against results obtained by van den Bogert (2016). These benchmarks are documented in Appendix B.

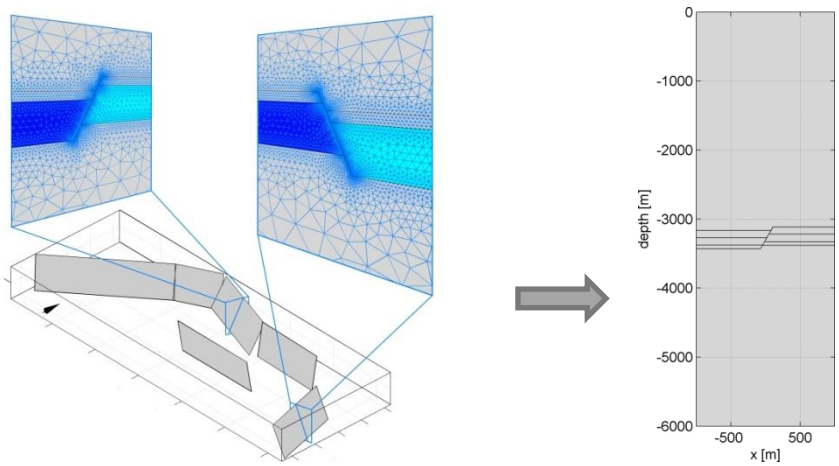

Figure 12: Sketch summarizing the model geometry.

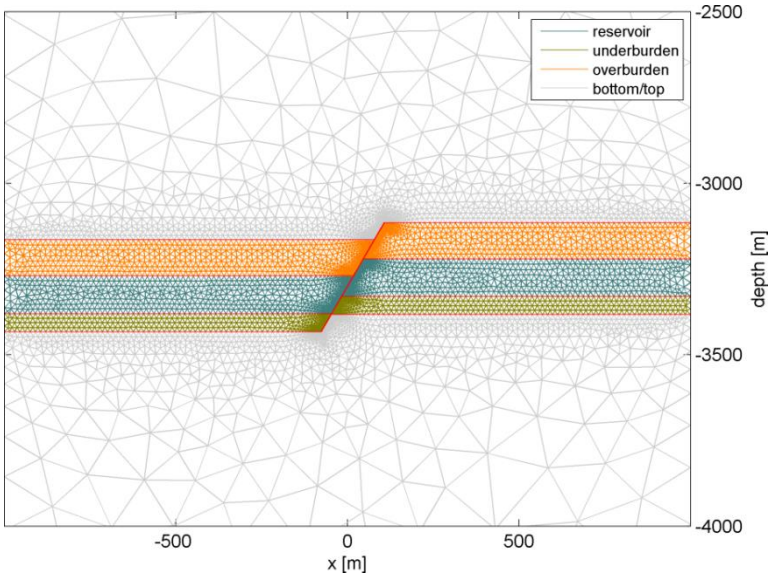

Figure 13: FEM-implementation of the reservoir geometry. Although over- und underburden layers were implemented in the model, these were extrapolated to the model boundaries. Mesh resolution along the fault is 0.1 m.

4.2.2 Smoothing of SCU

The geometrical model introduced in the previous section is prone to localized stress concentrations at the fault intersection with the top and bottom of the reservoir layer. The magnitude of these stress concentrations is depending on the spatial sampling. With a finer spatial sampling, the stress concentration becomes larger in amplitude but more localized.

To avoid bias from this model characteristic, the stress criticality (i.e. SCU) is smoothed along the fault on 10 m segments using a moving average filter (note: the sampling interval

on the fault is 0.1 m).

The filter length of 10 m is inspired by the lower magnitude detection threshold of the KNMI earthquake catalogue. Earthquakes with a characteristic slip length of less than 10 m (approximately corresponding to M_L <0 when assuming 2 MPa stress drop) would most likely not be detected by the KNMI station network.

Using a larger filter length of 35 m (corresponding to $M_L \approx 1$), we have confirmed that the results of this study are not critically depending on a specific choice of the filter length (Appendix C.2).

4.2.3 Principal stresses

In the current approach, the stress field is considered an 'unconstrained' parameter which is derived as part of the calibration procedure (section 4.3).

Since effective stress ratios of horizontal stresses to vertical stress are part of the final model parameter set, only the vertical principal stress needs to be defined ahead of the simulation runs. Here, an example from a stress model used by (2013) has been adopted. This model is based on well logs in the Bergermeer reservoir with a lithostatic gradient (S_v) of 23 MPa/km. The horizontal principal stresses are given by the respective *k*-ratios defined as

$$k_{Sh,SH} = \frac{S_{h,H} - p}{S_v - p} \qquad \textit{Equation 2}$$

where *p* is fluid pressure and $S_{h,H}$ are the minimum and maximum horizontal, principal stresses. It has to be noted that the specific selection of a vertical stress gradient finally determines the value of *k*-ratios derived in the calibration procedure. However, with the absolute shear and normal stresses on a fault predominantly depending on differential stresses of vertical and horizontal principal stresses (not considering fault orientation), any variation in S_v will only be reflected in a corresponding variation of *k*-ratios without changing the simulation results. Hence, the specific selection of S_v is considered to have no significant impact on the principal results of this study.

4.2.4 Fluid pressure

In the numerical model, a pressure gradient of 10 MPa/km outside the reservoir layer and a gas gradient of 2 MPa/km inside the reservoir layer are assumed (Figure 14).

Initial simulations demonstrated that sealing faults play a more important role than assumed in previous studies. E.g. van den Bogert (2016) assumes that in situ fluid pressure inside a sealing fault is the same as within (one side of) the reservoir. Therefore, the fault stabilizes during depletion and large poro-elastic stress changes are required to make the fault overcritical. From a geomechanical perspective, alternative assumptions are reasonable, i.e. the sealed (impermeable) core is assumed to be the slipping area. The dominating impact of sealing faults was noted in similar studies (van Wees et al., 2017). For the current study, a hydraulically isolated fault outside non-overlapping parts of the reservoir layer is assumed (Figure 15).

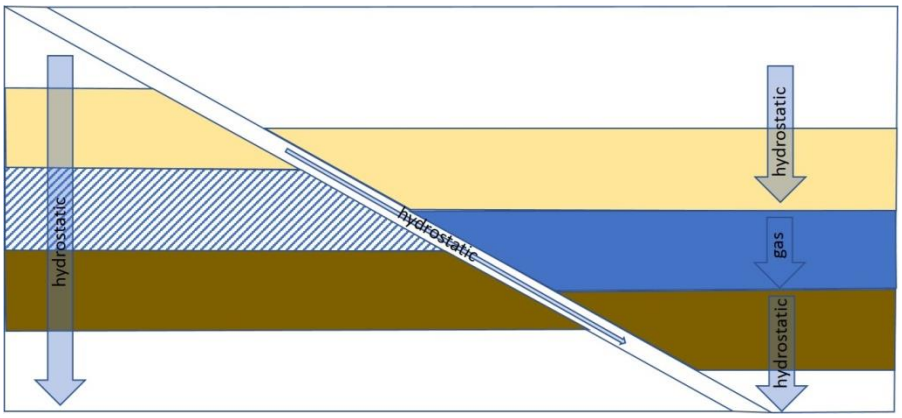

Figure 14: Sketch showing fluid pressure gradients in the numerical model.

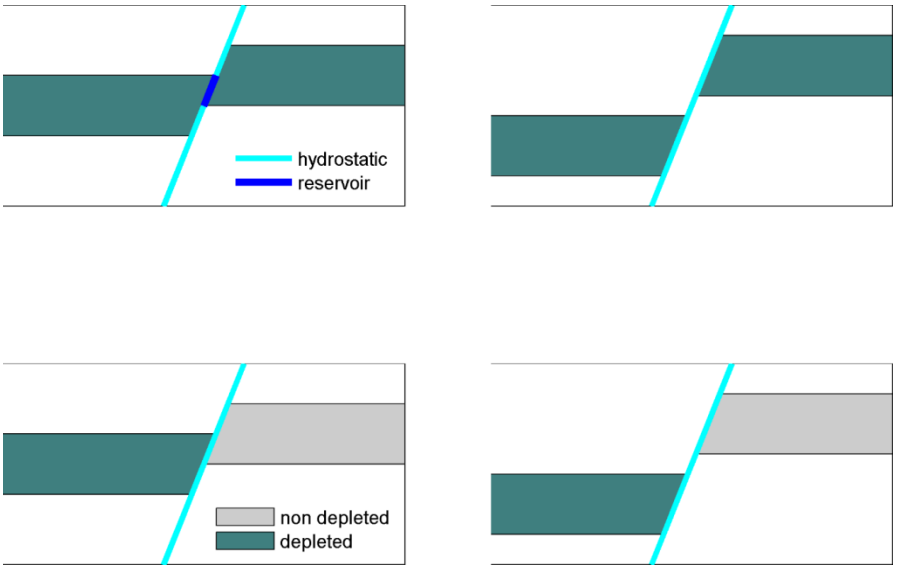

Figure 15: Sketch showing the fluid pressure inside an internal fault (top) and inside a boundary fault (bottom). For internal faults, two-sided reservoir depletion is assumed, for boundary faults, 1-sided depletion only (either in the foot wall or the hanging wall) is assumed. In case of overlapping segments of reservoir layers on both sides of an internal fault, pressure inside the fault (dark blue line) is identical to the pressure in both sides of the reservoirs, including the current level of depletion.

4.2.5 Elastic parameters

In the main database, elastic parameters are not stated as a single value but in terms of a parameter range. Sensitivity tests were performed to investigate if the results of the calibration procedure are depending on a specific parameter value chosen from the parameter range. For these tests, minimum, maximum and average parameter values were chosen. The overall numerical simulation results, however, do not exhibit systematic differences. Hence, average parameter values were selected for subsequent numerical

simulations.

4.2.6 Fixed global parameters

In addition to the ‘constrained’ and ‘unconstrained’ model parameters, several parameters were fixed *a priori*. It is assumed that these fixed parameters are reasonably constrained and do not (significantly) vary over The Netherlands. Associated parameters are summarized in Table 3.

parameter		value
vertical stress gradient	$\Delta SV/\Delta z$	23 MPa/m
hydrostatic gradient	$\Delta p/\Delta z$	10 MPa/km
gas gradient	$\Delta p/\Delta z$	2 MPa/km
Biot coefficient	α	0.8

Table 3: Fixed global model parameters.

4.2.7 Automated simulation

To cope with the large number of simulations and models required to conduct this study, an automated simulation chain has been set up. This includes the automated generation and meshing of a reservoir model within the simulation software. In a scripting environment, a range for the ‘unconstrained’ parameter under investigation can be entered and the simulation procedure is invoked. Utilizing the main database interface, the output is the state of criticality for all individual faults in the reservoirs contained in the main database.

4.3 Calibration procedure

In a calibration procedure, an optimized set of ‘unconstrained’ parameters is identified, yielding the best agreement between simulated stress criticality and observed seismicity (‘match’). Initially, unconstrained parameters were assumed globally, i.e. the same set of unconstrained parameters is assumed for all reservoirs. Table 4 lists the unconstrained parameters. As a requirement in the calibration procedure, only those parameter combinations were considered which yield overcritical stress conditions for all category A (‘most likely associated with seismicity’) reservoirs. By this requirement, numerical simulations tend to be conservative in the sense that all reservoirs which were actually associated with induced seismicity are also ‘simulated’ to respond seismically. Mismatch between simulations and observations are restricted to gas fields which are not associated with induced seismicity (‘over prediction’).

In principle, a perfect match with observations can be obtained by allowing reservoir specific variations of the unconstrained parameters (i.e. introducing a large number of free model parameters). For example, all seismically active reservoirs could be assigned a low fault stability in order to match observations with hindsight. This approach, however, is of limited

use for assessing a future seismicity response. Therefore, a single, global (i.e. NL-wide) set of ‘unconstrained’ parameters would be the ideal outcome of the calibration procedure (‘minimum complexity model’).

The calibration procedure is outlined in (Figure 16). For a specific combination of ‘unconstrained’ parameters, a simulation run is started, iterating over all reservoirs and its respective faults. The state of stress on a fault before and after depletion (either as of 2017 for category D reservoirs, or at the onset of seismicity for category A reservoirs) is computed.

Simulation runs were evaluated based on the number of reservoirs matching observation data with a specific combination of ‘unconstrained’ parameters. For category A reservoirs, a match is considered if overcritical stress conditions are simulated on at least one reservoir fault. For category D reservoirs, a match implies that subcritical conditions are simulated for all reservoir faults.

An unconstrained parameter combination is rejected in case over-critical stress conditions are simulated prior to depletion for at least one reservoir fault. Furthermore, all parameter combinations which do not provide a match for the entire set of category A reservoirs are rejected.

parameter	
faults	throw
	dip
	stability (coefficient of friction, cohesion)
stress field	trend SH
	k_{Sh}
	k_{SH}

Table 4: List of unconstrained parameters.

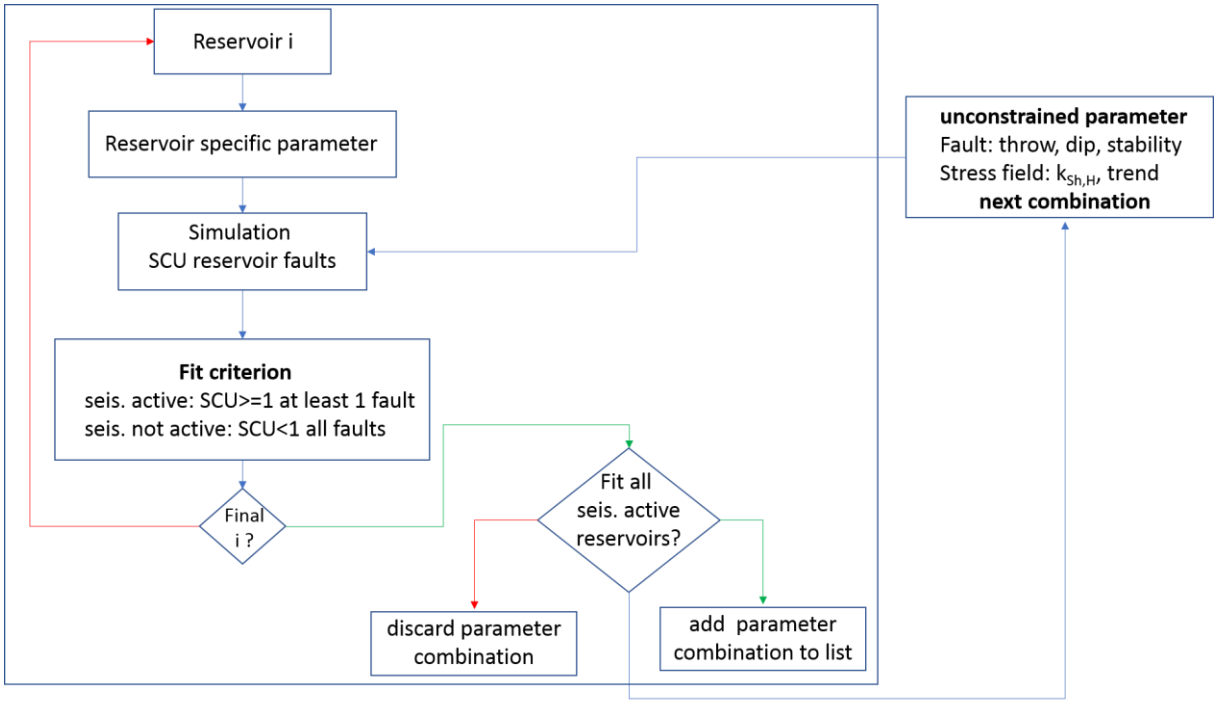

Figure 16: Flowchart of the calibration procedure to identify the best fit model. Red arrows denote a 'No' branch, green arrows a 'Yes' branch.

4.4 Calibration results

4.4.1 Minimum complexity model

The rationale behind minimizing the degrees of freedom in the calibration procedure has been explained in 4.3. In the minimum complexity model, a global set of unconstrained parameters is assumed. More precisely, it is assumed that a suitable model with constant values for stress field and unconstrained fault parameters can be identified which is valid all over the Netherlands.

Table 5 lists the range considered for each 'unconstrained' parameter. Possible parameter combinations were systematically investigated over the entire parameter range resulting in several 100,000 numerical models.

The parameter combination BFM-G resulting in the largest number of matches is listed in Table 6. For this parameter combination, all 12 category A reservoirs are simulated to produce seismicity and 11 category D reservoirs to not produce seismicity (corresponding to 28%). This set of parameters, however, is not according to what is expected regarding average fault throw and dip for onshore gas fields in the Netherlands. Hence, the parameter range around an expected value of fault throw = 100 m and dip = 70° has been re-scanned. This resulted in the alternative model BFM-P as listed in Table 7. BFM-P yields a match for all category A reservoirs and 10 category D reservoirs (corresponding to 26%). Associated SCU values are shown in Figure 17.

It should be noted, that the category D reservoirs matched with BFM-P are a subset of those matched by BFM-G. Similarly, alternative parameter combinations yielding the same number of matches as BFM-P also match the same reservoirs (compare Appendix C.1).

This demonstrates that the constrained reservoir parameters indeed carry information about whether or not a gas field responds seismically to gas production. Despite making global assumptions regarding the unknown parameters, this information can at least partly be extracted by the proposed workflow.

parameter	range
throw	25m – 250m
dip	55°-80°
μ	0.4 – 0.9
k_{Sh}	0.3 – 0.685
k_{SH}	0.85
trend SH	90°- 270°

Table 5: Range of unconstrained parameters investigated in the calibration procedure. Note: For any chosen value of μ, fault cohesion C_0 is implicitly determined by the assumption of fault stability prior to gas production (the smallest C_0 fulfilling this requirement is chosen). Note also: sensitivity tests revealed that the simulation results are not critically depending on the value of k_{SH}.

parameter	value
throw	250 m
dip	55°
μ	0.8
C_0	0 MPa
k_{Sh}	0.3075
k_{SH}	0.9
trend SH	120°

Table 6: Unconstrained parameters for the minimum complexity model BFM-G resulting in 100% category A matches and 28% category D matches.

parameter	value
throw	100 m
dip	70°
μ	0.8
C_0	1.93 MPa
k_{Sh}	0.3
k_{SH}	0.85
trend SH	120°

Table 7: Unconstrained parameters for the minimum complexity model BFM-P resulting in 100% category A matches and 26% category D matches.

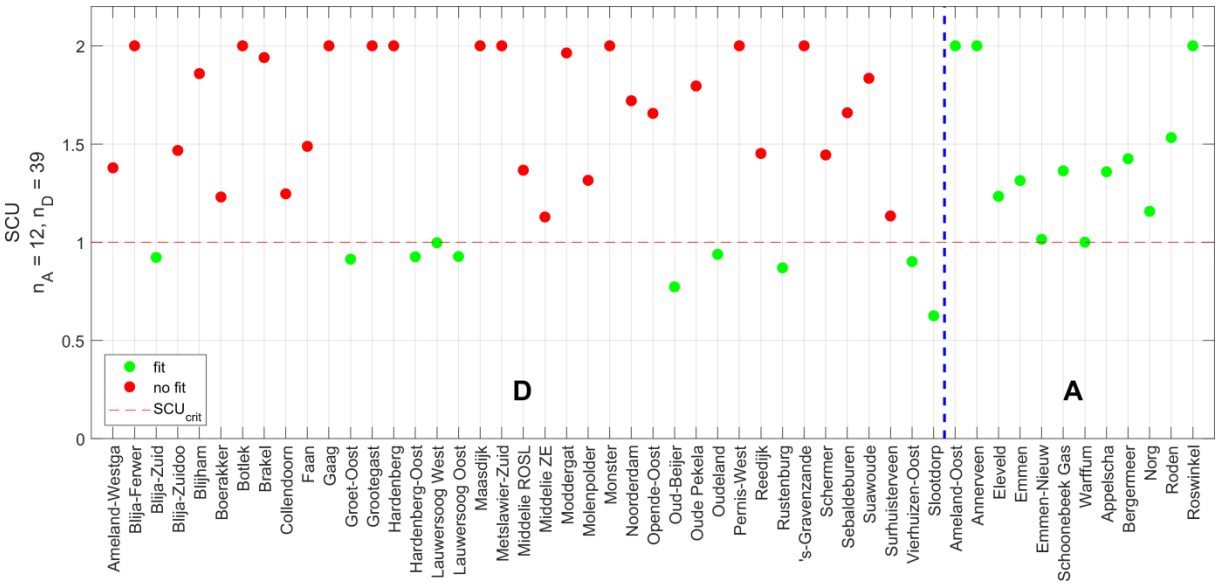

Figure 17: Numerically simulated SCU values based on the BFM-P model for all reservoirs. Dashed blue line separates category D from category A reservoirs. Green colours indicate match, red colours indicate mismatch. SCU-values have been saturated at a level of 2 for displaying purposes.

4.4.2 Reservoir specific k_{Sh}

Given the low percentage of matches obtained with the minimum complexity model BFM-P, several options for increasing the number of (free) model parameters were considered. A potential candidate for such a parameter is the presence of salt overlaying the reservoir. In previous analyses, it was suspected that salt could lead to a lower k_{Sh} value (e.g. Fredrich et. al, 2003).

Salt layers are associated with most Rotliegend reservoirs, which are either the Rotliegend or the Slochteren formation in the main database. An exception is the Bergermeer reservoir that is not associated with salt layers of significant thickness (e.g. Nieuwland et al., 2011). Rotliegend reservoirs are confined to the North of the Netherlands (Figure 18).

In a separate simulation run, BFM-P model parameters were assumed for Rotliegend reservoirs and a higher k_{Sh} value of 0.8 for was assumed for the other reservoirs. With this strategy, k_{Sh} is treated as a constrained, reservoir specific parameter (switching between two values).

Simulation results demonstrate that the mandatory condition of matching all category A reservoirs could not be achieved with this approach (Figure 19). Hence, this approach has been discarded.

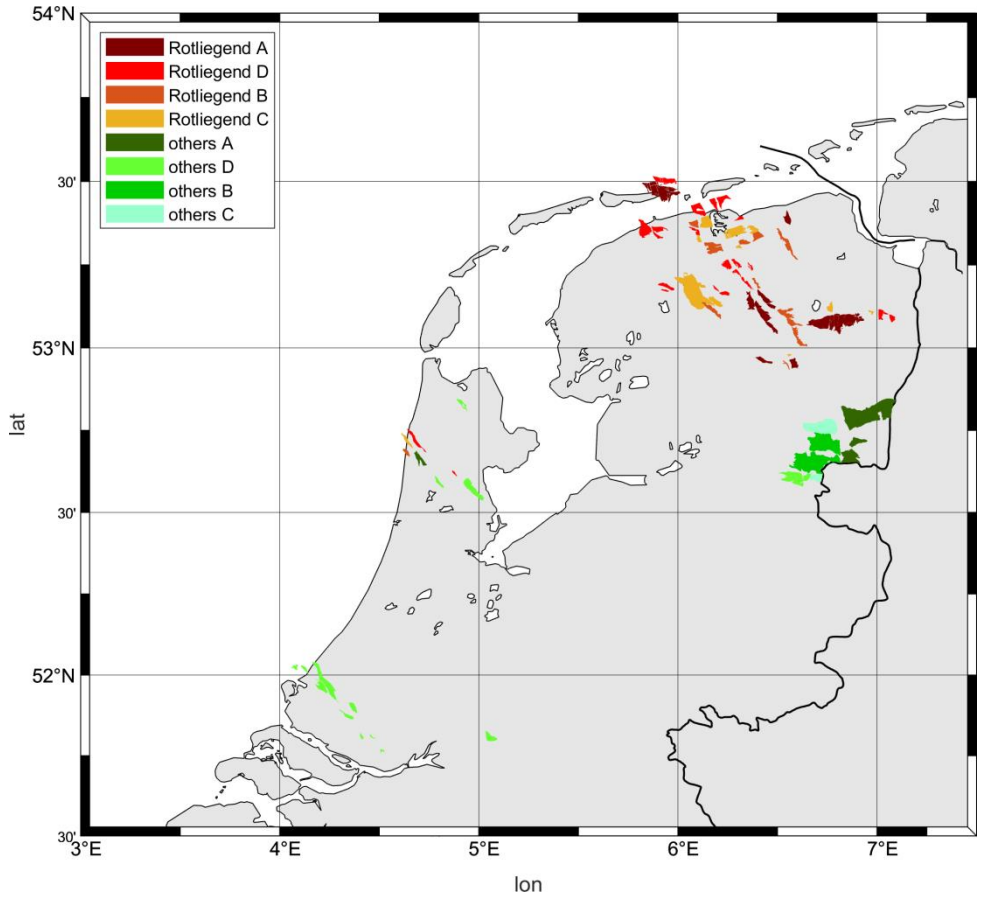

Figure 18: Overview of the spatial distribution of Rotliegend and non-Rotliegend reservoirs considered in this study. Rotliegend reservoirs are depicted in red, non-Rotliegend in green colours. Colour graduation denotes different reservoir categories according to figure legend.

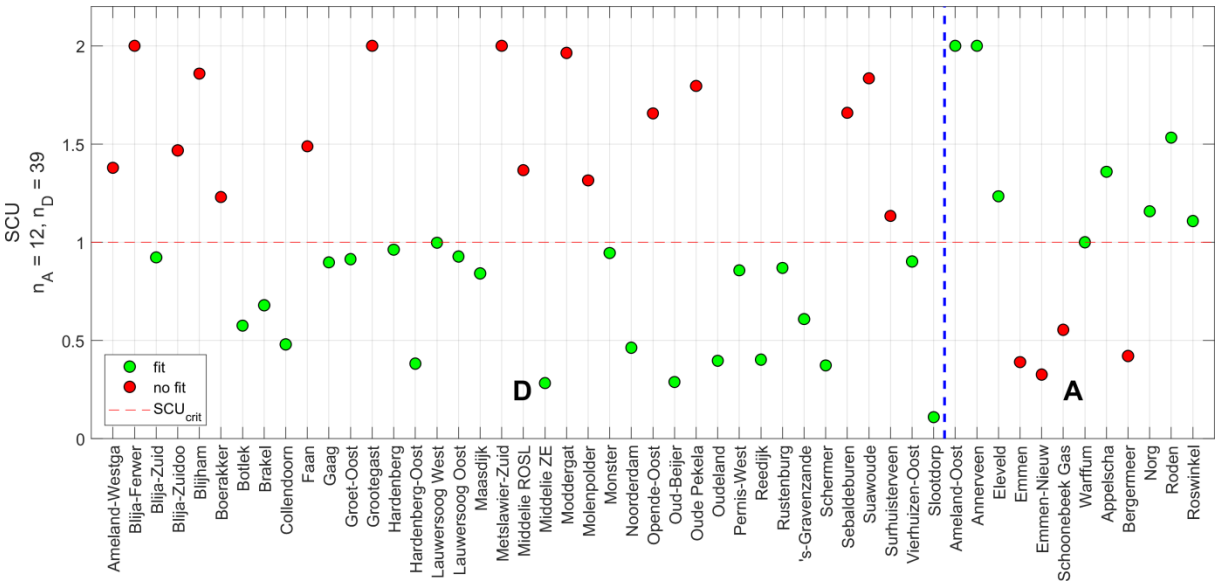

Figure 19: Numerically simulated SCU values based on the BFM-P model with a different k_{Sh} value for non-Rotliengend reservoirs. Dashed blue line separates category D from category-A reservoirs. Green colours indicate match, red colours indicate mismatch. SCU-values have been saturated at a level of 2 for displaying purposes.

4.4.3 Regional k_{Sh} (BFM-SW)

An alternative option for introducing an additional (free) model parameter is based on the observation that mismatches of category D reservoirs systematically prevail in the South-West of The Netherlands.

Considering the Roer-Valley rift system separating the South-West of the Netherlands from the North, it is plausible that geomechanical parameters could be different in the South-West compared to the North. In principle, this might be true for any of the 'unconstrained' parameters. In the subsequent model we focus on the k_{Sh} parameter, which is assumed to be higher in the South-West. We note, however, that the same results can be obtained when allowing any other of the unconstrained parameters to be different in the South-West.

Keeping parameters of the BFM-P model and assigning a higher k_{Sh} value to the reservoirs located in the South-West (compare Figure 20 and Table 8), the numerical simulations result in a 100% match of category A reservoirs and 49% match of category D reservoirs.

With this result, the BFM-SW model is the preferred model developed in this study.

parameter	value	
	SW	rest
throw	100 m	100 m
dip	70°	70°
mu	0.8	0.8
C_0	1.93 MPa	1.93 MPa
k_{Sh}	0.8	0.3
k_{SH}	0.85	0.85
trend SH	120	120

Table 8: Unconstrained parameters for the minimum complexity model BFM-SW resulting in 100% category A matches and 49% category D matches.

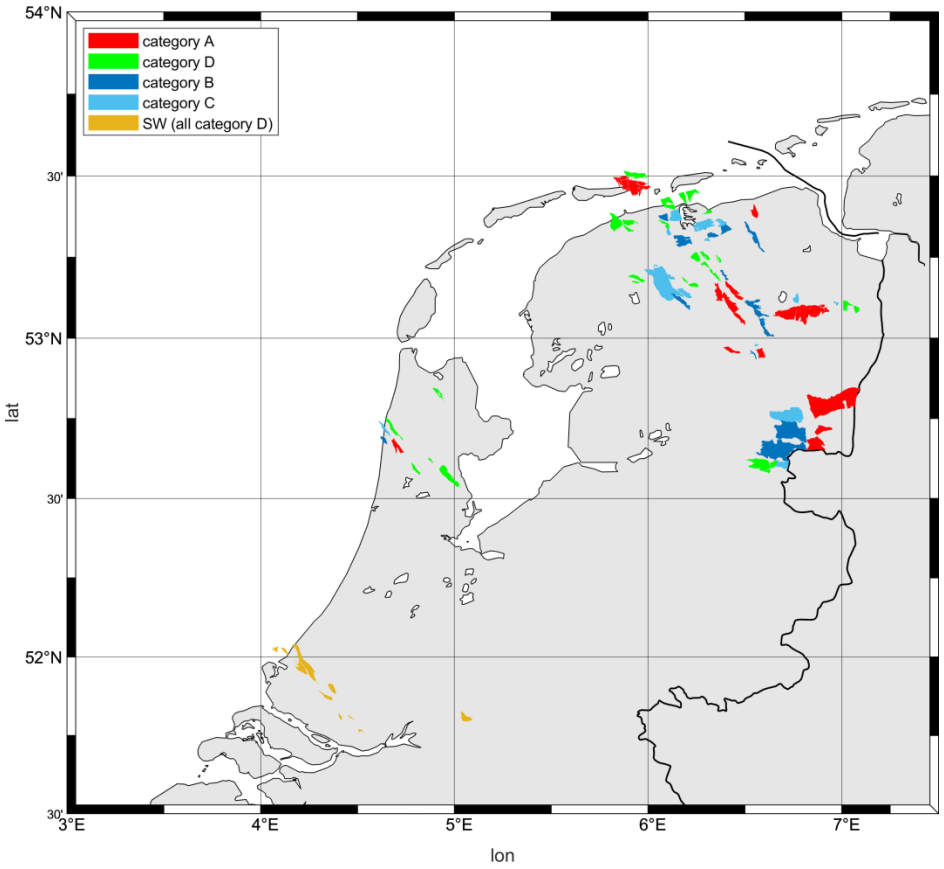

Figure 20: Overview of the spatial distribution of categories for the reservoirs considered in this study. Fields in the South-West of the NL are coloured in orange, all of which are of category D.

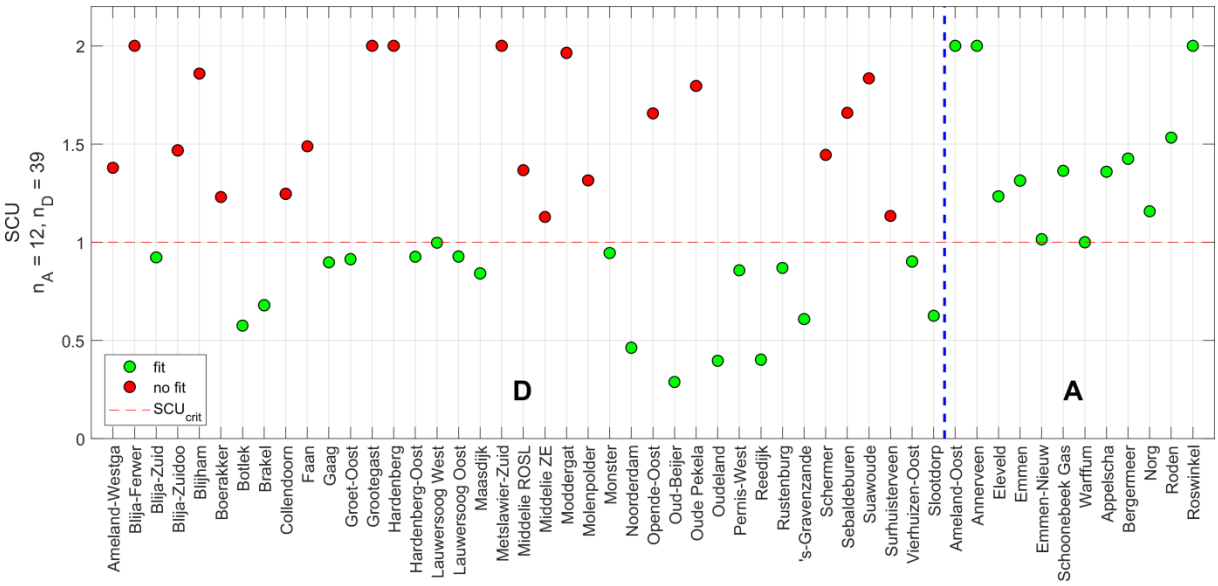

Figure 21: Fit-statistics for the model with regional variation of unconstrained parameter. At least one fault has been simulated as overcritical in all 12 category A reservoirs, while all faults in 19 category D reservoirs resulted in a non-critical state of stress. Dashed blue line separates category D from category A reservoirs. SCU-values have been saturated at a level of 2 for this display.

4.5 Consistency test category B, C reservoirs

Until here we have focussed on matching observations from category A ('most likely associated with induced seismicity') and category D reservoirs ('most likely not associated with induced seismicity'). Observation data from category B and C reservoirs ('possibly associated with seismicity') has not been considered due to the uncertainty associated with observation data.

Although category B and C reservoirs cannot be used in the calibration procedure described above, the earthquake observations associated with these reservoirs nevertheless carry important information: Consider a single earthquake that is either associated with reservoir X or reservoir Y. Here we would expect that overcritical stress conditions are simulated for at least one of the two reservoirs.

Using our preferred model BFM-SW (Table 8) we have performed the following consistency test. For all 1,774 earthquakes associated with gas production in The Netherlands (KNMI catalogue as of January 2018) we have investigated whether or not at least one overcritical reservoir is simulated within 2.5 km distance (taken as a proxy for the location uncertainty). Since the earthquake catalogue also includes Groningen seismicity, the Groningen reservoir was included as a category A reservoir (although not included in the numerical simulations).

To reduce computational effort, the numerical simulations are based on the depletion level stated in the main database. This is not strictly correct since for category B reservoirs, the depletion level in the database refers to the occurrence time of the first earthquake. Whereas the depletion level for category C reservoirs refers to the depletion as of 2017. For the

consistency test, however, we feel that this approximation is acceptable. A more detailed analysis accounting for all possible combinations was not feasible in the context of this study.

The consistency test revealed that all but 3 earthquakes are explained by the BFM-SW model (Figure 22) allowing for 2.5 km lateral location uncertainty. These 3 earthquakes, however, cannot be associated with any gas reservoir within 2.5 km distance. Therefore, these earthquakes do not indicate inconsistency.

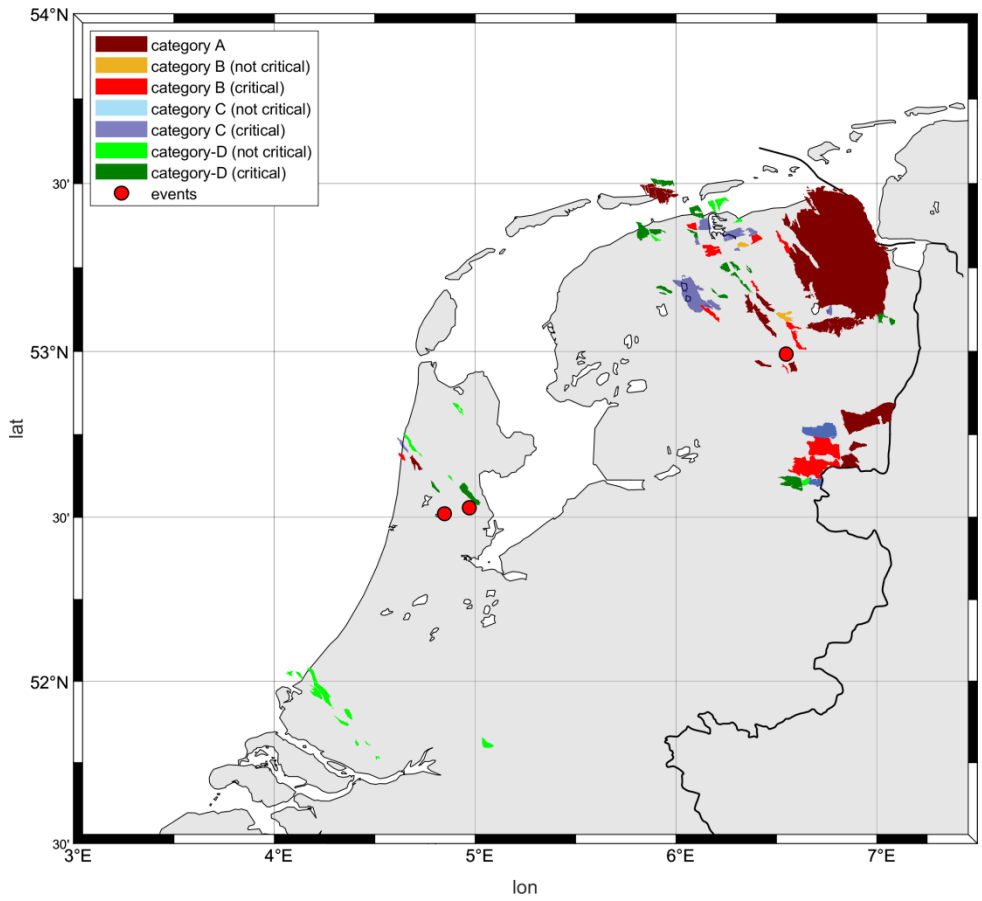

Figure 22: Epicenters of the events that could not be matched by BFM-SW (red dots). All reservoirs considered in the study are displayed, with the Groningen field additionally included for this investigation. Colour code of the reservoirs corresponds to reservoir category according to the legend.

4.6 Seismicity prognosis

Using the BFM-SW model, a prognosis of future seismic response of category D reservoirs at the end of the reservoir lifetime is performed. The objective is to determine how many additional reservoirs become seismically active. To this end, the final depletion level of reservoirs was provided by SodM (SodM 2018d) and missing data have been set assuming a general leaving pressure of 20 bar (Figure 23). The simulation results predict 10 category-D reservoirs to produce no seismicity during their lifetime (Figure 24).

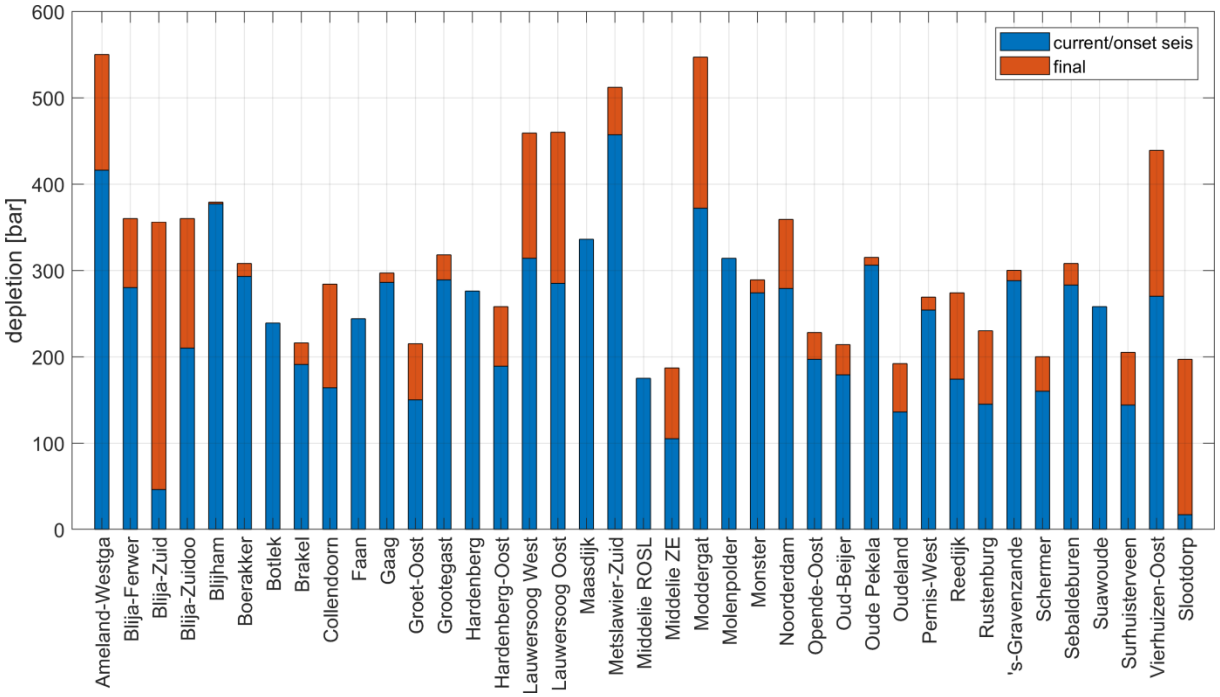

Figure 23: Depletion level (current or at onset of seismicity) and predicted future depletion until the end of the lifetime of the reservoirs. Only category D reservoirs are considered.

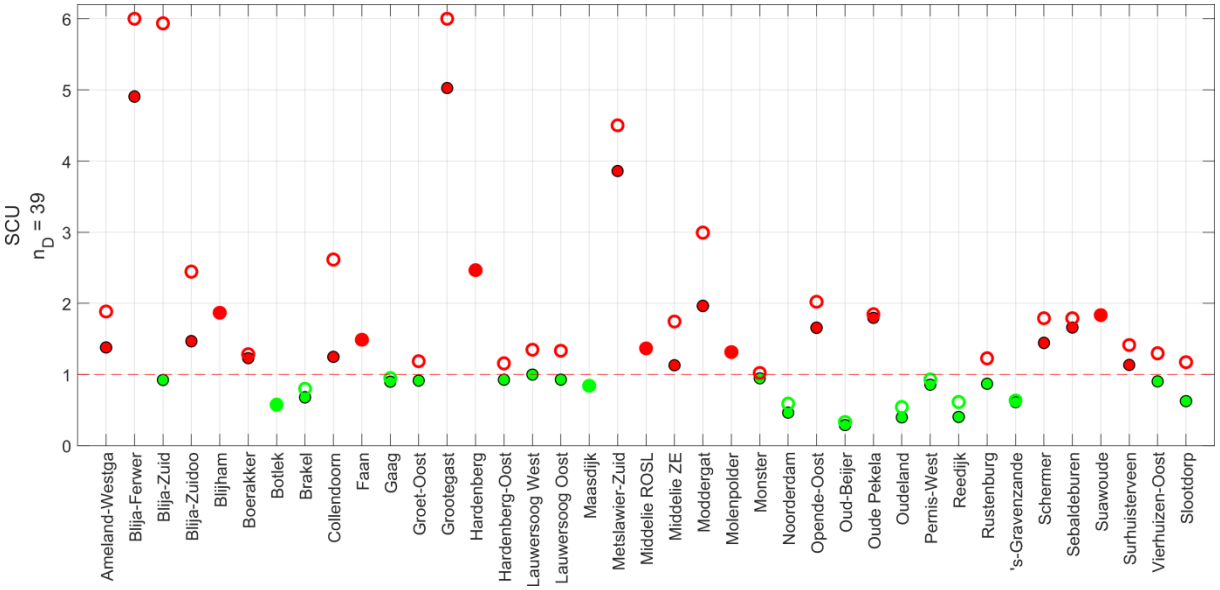

Figure 24: Prediction of future seismic activity for category-D reservoirs. Current SCU (filled circles) and SCU level at the end of the reservoir lifetime (open circles).

4.7 Comparison with DHAIS

Assessment of the seismic hazard associated with gas production in The Netherlands is currently based on a deterministic hazard analysis scheme (DHAIS) proposed by van Thienen-Visser et al. (2012).

DHAIS includes four parameters. The probability P for the occurrence of seismicity in a gas reservoir, relative pressure depletion, the ratio of fracture surface to reservoir volume B and the Young's modulus ratio between reservoir and burden E. The latter three parameters are utilized in calculating P.

DHAIS values were provided by SODM (van Thienen-Visser et al., 2012, extended confidential version) for comparison with our study results. Figure 25 to Figure 27 show this comparison for the reservoirs used in the calibration procedure.

The DHAIS values also exhibit a considerable number of mismatches in the sense that either a seismically active reservoir of category A was assigned a low probability for earthquakes or a category D reservoir was assigned a high probability. The DHAIS mismatches, however, seem to be uncorrelated with the mismatches obtained with the physics-based approach.

Finally, prediction of future seismic activity at the end of the reservoir's lifetime has been compared to DHAIS (Figure 28-Figure 30) as well as Young's modulus ratios between overburden and reservoir (Figure 31).

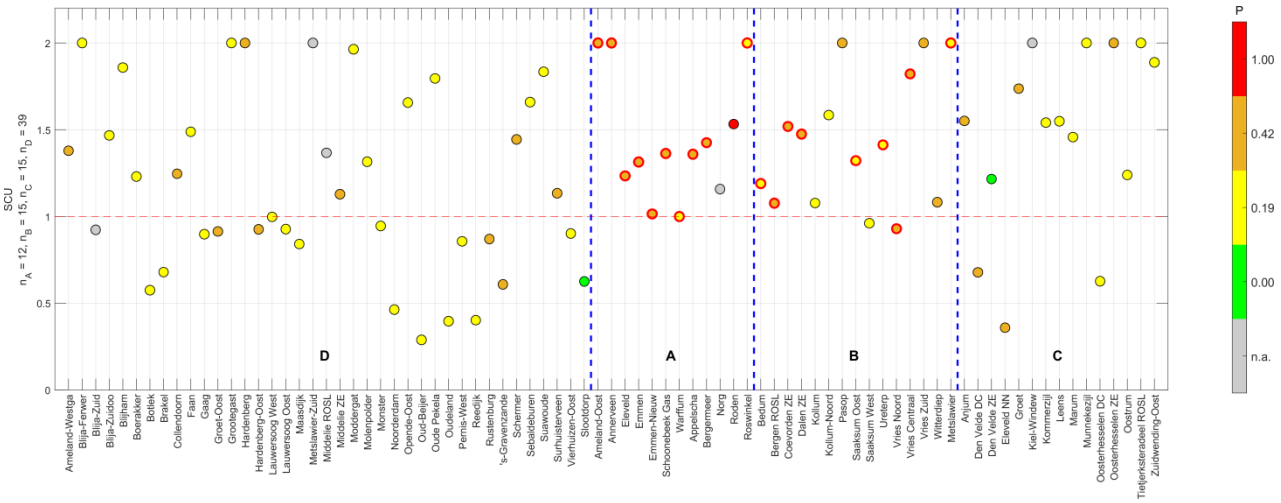

Figure 25: Comparison of BFM-SW model results with DHAIS parameter P according to the colour map. Reservoirs with no P value available are denoted by grey circles. Red open circle denotes those reservoirs where the computed P value was overwritten by P=1 accounting for the fact, that the reservoir already produced seismicity. SCU-values are saturated at a level of 2 for displaying purposes. Dashed blue line separates reservoir categories.

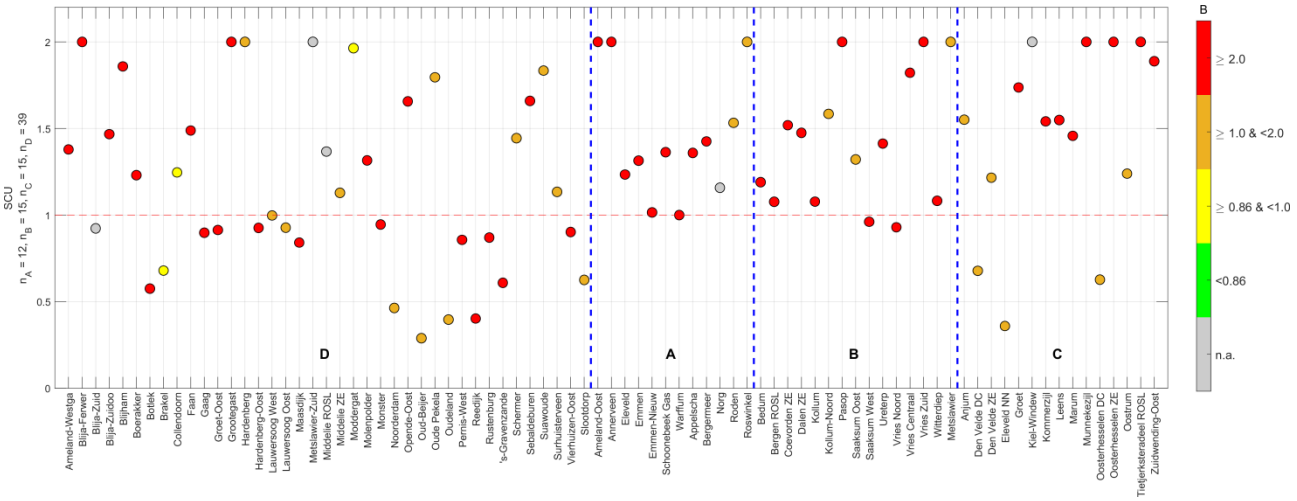

Figure 26: Comparison of BFM-SW model results with DHAIS parameter B according to the colour map. Note that no reservoirs with B-values below 0.86 are in the main database. Reservoirs with no B value available are denoted by grey circles. SCU-values are saturated at a level of 2 for displaying purposes. Dashed blue line separates reservoir categories.

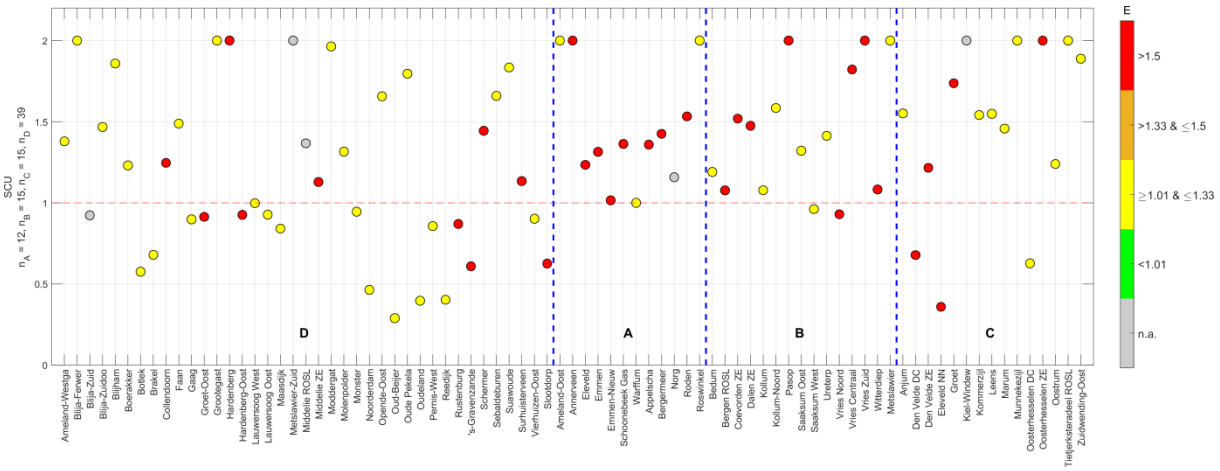

Figure 27: Comparison of BFM-SW model results with DHAIS parameter E according to the colour map. Note that no reservoirs with E-values below 1.01 and between 1.33 and 1.50 are in the main database. Reservoirs with no E value available are denoted by grey circles. SCU-values are saturated at a level of 2 for displaying purposes. Dashed blue line separates reservoir categories.

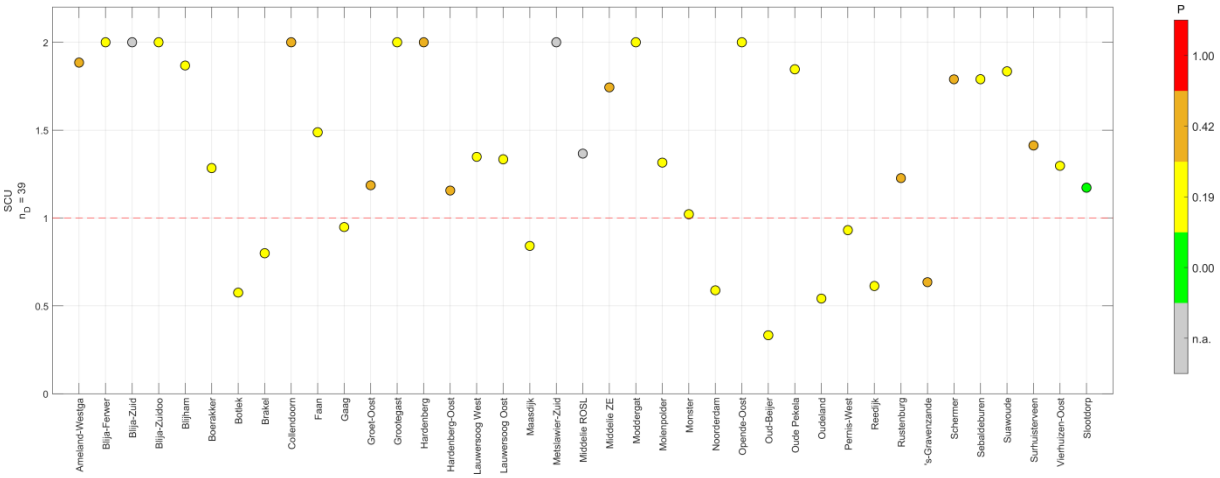

Figure 28: Comparison of BFM-SW model prediction of future seismicity for category D reservoirs with DHAIS parameter P. Reservoirs with no P value available are denoted by grey circles. SCU-values are saturated at a level of 2 for displaying purposes. Dashed blue line separates reservoir categories.

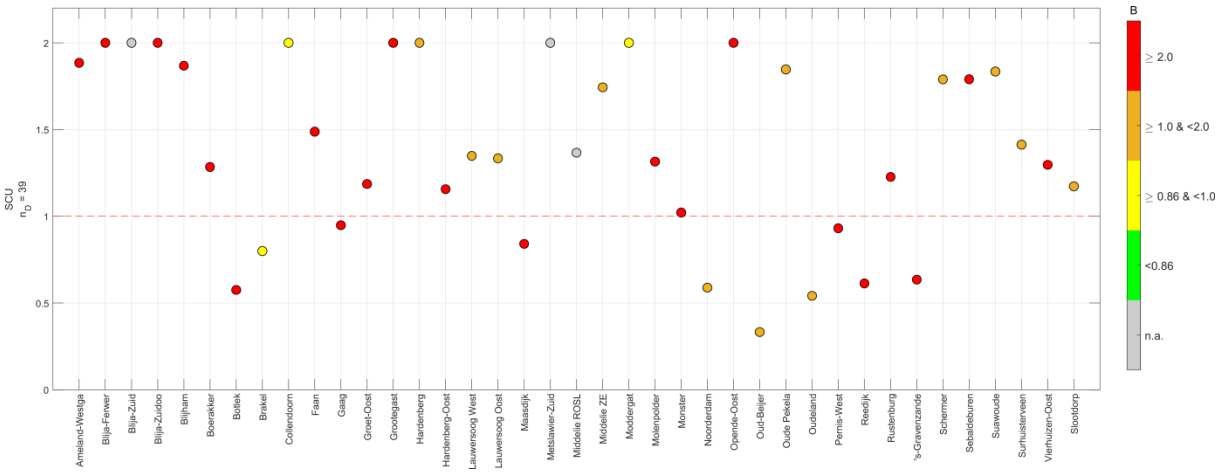

Figure 29: Comparison of BFM-SW model prediction of future seismicity for category D reservoirs with DHAIS parameter B. Reservoirs with no B value available are denoted by grey circles. SCU-values are saturated at a level of 2 for displaying purposes. Dashed blue line separates reservoir categories.

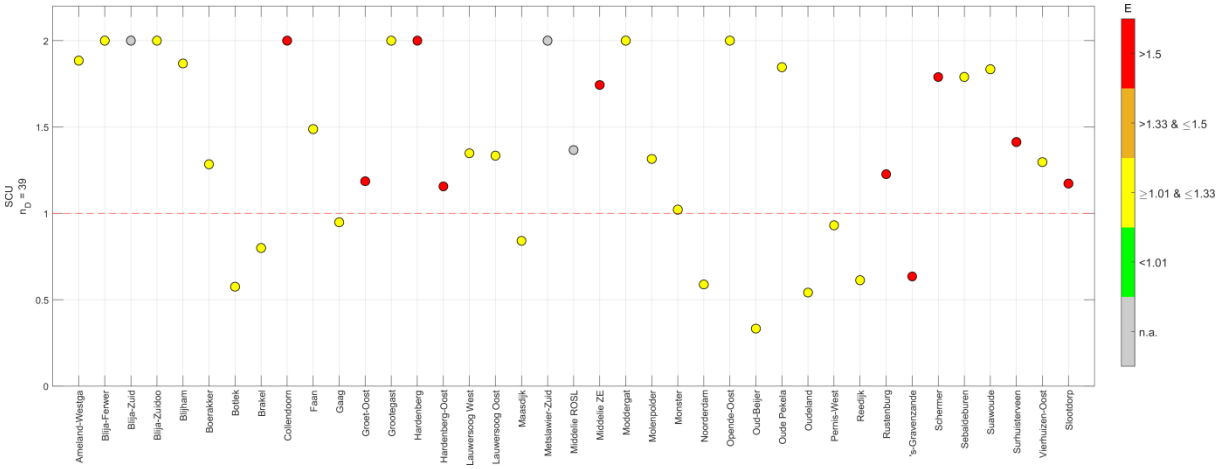

Figure 30: Comparison of BFM-SW model prediction of future seismicity for category D reservoirs with DHAIS parameter E. Reservoirs with no E value available are denoted by grey circles. SCU-values are saturated at a level of 2 for displaying purposes. Dashed blue line separates reservoir categories.

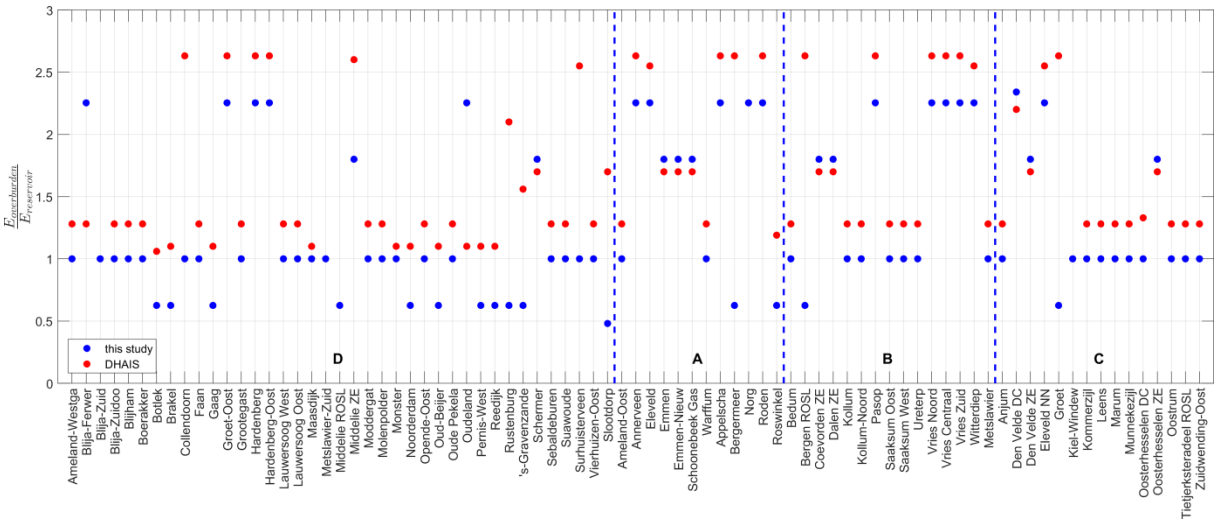

Figure 31: Comparison of Young's modulus ratio between overburden and reservoir in this study and DHAIS, separated according to reservoir category.

5 DISCUSSION

The guiding question addressed with the current study is why seismicity has occurred in certain gas fields, whereas other gas fields remained seismically quiet. With the physics-based numerical simulation framework developed in this study, we have found indications that the seismicity response to gas production is indeed determined by a small set of parameters which in principle can be assessed prior to gas production. Starting from a minimum complexity modelling approach, those subsurface parameters which were not constrained by observation data were addressed by global assumptions. Using a combination of reservoir specific and globally assumed parameters, the observed seismicity response could be matched for all seismically active fields (category A) and for up to 50% of the seismically inactive fields. An equally good match was obtained for different constellations of globally assumed parameters, reflecting the multi-parameter nature of the induced seismicity phenomenon. Importantly, observation matches for the different parameter constellations tend to be obtained for the same category A and D gas fields, demonstrating that the reservoir specific parameters carry significant information about the seismicity response to gas production. Concerning the main research question our findings indicate that

- the seismicity response of the gas fields can be described by Coulomb stresses simulated with simple numerical models,
- the sign of Coulomb stresses[1] is determined by parameter combinations rather than by a single parameter. Alternative parameter combinations can yield the same level of Coulomb stresses and we did not see any obvious correlation with a single reservoir parameter.

The latter finding demonstrates fundamental limitations of those approaches making a seismicity prognosis based on empirical key parameters.

To further study the modelling performance of our physics-based approach, we have chosen a preferred set of global parameters (model 'BFM-SW'). The BFM-SW model parameters need to be envisaged as a parameter ensemble, where individual parameter values can be changed as long as the ensemble 'characteristics' remains the same. E.g. reducing fault friction while at the same time increasing fault cohesion can lead to the same (ensemble) fault strength. Therefore, individual parameter values of the BFM-SW model should not be interpreted outside the context of the current study.

For assessing induced seismicity hazard, the BFM-SW model already provides important constraints for those gas fields, for which no seismicity is forecasted[2]. On the other hand, BFM-SW significantly over-predicts the seismicity response, i.e. 50% of the gas fields for which seismicity is forecasted are not (yet) associated with earthquakes. We see, however, potential for improving the forecasting capabilities of the framework developed here. Besides increasing the complexity of the geometrical model, reducing parameter uncertainty is a

[1] positive Coulomb stresses imply failure, negative values imply no seismicity
[2] The BFM-SW model is conservative in the sense that none of the gas fields that have (historically) produced seismicity is 'forecasted' to remain seismically quiet.

candidate for improvement. In particular, replacing global assumptions on fault dip and fault throw, as currently done, by reservoir specific values is expected to have a first order impact. Further improvements could possibly be achieved by including information on earthquake strength into the simulation framework.

We see the potential that a physics-based framework can eventually become part of the standard seismic hazard assessment for small gas fields in The Netherlands. With the current study, we have demonstrated the feasibility of this type of approach. Future work, however, is required before the approach can be applied in practise. Furthermore, the 'prediction power' of the approach is not yet tested as the model framework was calibrated using the entire set of observation data. Ideally, this data set should be split into two subsets used for 'training' (calibration) and for 'testing'. This, however, was not possible due to the small number of observation data.

REFERENCES

Fekkes, F., 2016. ‘Field Data Correlation of Reservoir Compaction and Seismic Potential of Dutch Onshore Gas Fields’, Master thesis, Faculty of geosciences, Utrecht university.

Fredrich, J.T. et al., 2003. ‘Stress Perturbations Adjacent to Salt Bodies in the Deepwater Gulf of Mexico‘, SPE 84554 conference paper.

, G., 2017. ‘Draft Results: Induced seismicity (or lack of it) in small fields in the Netherlands’, internal study SodM.

Nieuwland et al., 2011. ‘Structural Geometry of the Bergermeer Gas Field. Implications for induced earthquake magnitudes’. TAQA Energy.

SodM 2018a, Excel spreadsheet ‘parameters_DHAIS_voorSodM.XLS’, provided by SodM.

SodM 2018b, Excel spreadsheet ‘2018048 Norg Grijpskerk reservoir pressure taken from Dynamic Model’, provided by SODM.

SodM 2018c, Excel spreadsheet ‘DOMUS-#18054090-v1-GIIP informative onshore gasvelden’, provided by SODM.

SodM 2018d, Excel spreadsheet. ‘ProductieWinningsplannenPresure.XLSX’, provided by X. .

, P.A.J., 2015. , Impact of various modelling options on the onset of fault slip and the fault slip response using 2-dimensional Finite Element modelling’, NAM report.

, W., 2013. ‘Dynamic Geomechanical Modelling of the Bergermeer Underground Gas Storage, Netherlands’. Baker-Hughes report.

, et al., 2006. ‘Correlation between hydrocarbon reservoir properties and induced seismicity in the Netherlands’. Elsevier.

al., 2012. ‘Deterministische hazard analyse voor geinduceerde seismiciteit in Nederland’. TNO-rapport 2012 R10198.

et al., 2016. ‚Seismiciteit onshore gasvelden Nederland‘, TNO rapoort TNO 2016 R10164.

, J.-D., , P. A., , K., , B. B. T., , S., , B., , S. A., , L., and M. Pluymaekers, 2017. Geomechanical models for induced seismicity in the Netherlands: inferences from simplified analytical, finite element and rupture model approaches. Netherlands Journal of Geosciences, **96**, s183–s202.

APPENDIX A DATABASE

A.1. Database resources

	Resource	author(s) / provided by
1	Seismiciteit onshore gasvelden Nederland", TNO 2016 R10164, et al., 2016.	TNO
2	Draft Results: Induced seismicity (or lack of it) in small fields in the Netherlands, G. , 2017	SodM
3	parameters_DHAIS_voorSodM.XLS (EXCEL table containing, i.a., elastic rock parameter and pressure values of reservoirs).	SodM
4	DOMUS-#18054090-v1-GIIP_informatie_onshore_gasvelden.xlsx (EXCEL table containing GIIP values fo reservoirs)	SodM
5	2018048_Norg_Grijpskerk_reservoir_pressure_taken_from_Dynamic_Model.xlsx (EXCEL table with pressure data for reservoirs Norg & Grijpskerk)	SodM
6	Field Data Correlation of Reservoir Compaction and Seismic Potential of Dutch Onshore Gas Fields. F. Fekkes (2016).	MSc-thesis, University of Utrecht
7	nlog.nl (Winningsplan, information on wells etc.)	web resource, operated by TNO & the Dutch Ministry of Infrastructure and the Environment
8	dinoloket.nl (geological information on formations etc.)	web resource, operated by the Geological Survey of the Netherlands
9	Earthquake catalogue for the Netherlands (as of 24-1-2018)	KNMI

Table 9: Resources utilized for the setup of the main database.

A.2. Rock types and elastic parameter

layer	group	rock types	E [GPa]	ν [–]
reservoir	sandstone	sandstone claystone & sandstone & conglomerates sandstone & claystone sandstone & conglomerate sandy conglomerate siliciclastic sediments and, silt, coal and shale layers	18.9-25.7	0.23-0.28
	limestone	limestone dolomite limestone & dolomite	27.3-30.7	0.25-0.27
overburden	sandstone	sandstone sandstone & claystone sandstone & claystone & limestone sandstone & conglomerate conglomerate pebble conglomerate rock	24.9	0.25
	limestone	limestone	27.3	0.25
	anhydrite	anhydrite anhydrite & salt & claystone	52.2	0.29
	carbonates	carbonate carbonate & anhydrite carbonate & claystone & anhydrite carbonate (marl, dolomite, limestone)	49.5-51	0.29
	claystone	claystone	11.8-16.1	0.33-0.35
underburden	sandstone	sandstone & claystone sandstone & mudstone anhydritic sandstones and silty claystones	24.9	0.25
	anhydrite	anhydrite anhydrite & salt & claystone	52.2	0.29
	claystone	claystone claystone & salt silty claystone	11.8-16.1	0.33-0.35
	mudstone	mudstones silty mudstones silty to very fine-grained sandy mudstones	11.8-25.7	0.23 - 0.35
	marlstone	marlstone	11.8-51	0.23-0.35
	silicilastic sediments	fine-grained siliciclastic sediments (describes complete geology of Limburg group, may contain sandstones / mudstones / claystones)	covers complete range claystone-sandstone	covers complete range claystone-sandstone

Table 10: Classification of rock type for the different layers and corresponding elastic parameter range.

A.3. Reservoir depletion

For most reservoirs, depletion is provided in the primary data sources. In four cases, however, reservoir depletion had to be determined from the produced gas volume.

For the calculation of reservoir pressure at a specific time, the following equation was used (assuming a z-factor of 1):

$$\frac{p}{p_0} = \frac{GIP}{GIIP} \qquad \textit{Equation 3}$$

p_0 is the initial reservoir pressure, p the pressure at a given time. *GIP* (Gas In Place at time sample) can be determined utilizing the production data for the specific reservoir.

We compared calculated reservoir depletion to the depletion values stated in the primary data sources (Figure 32 and Figure 33) and obtain reasonable agreement for most reservoirs.

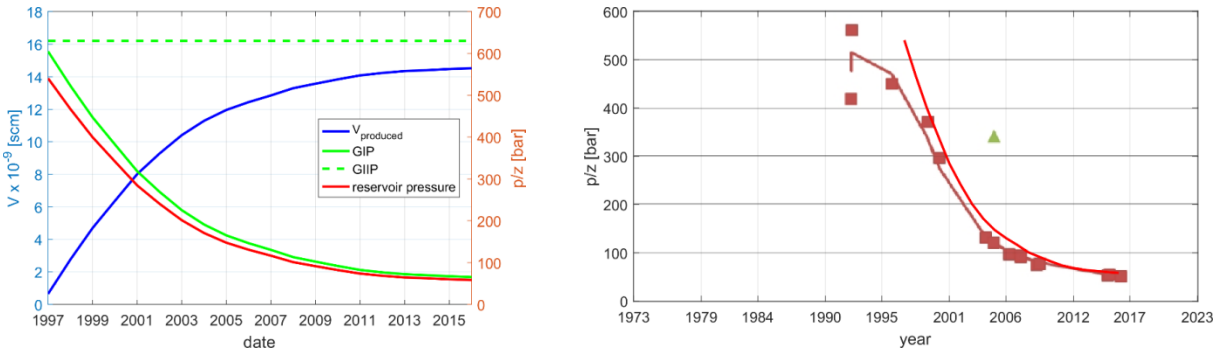

Figure 32: GIP and reservoir pressure as a function of time for the Anjum gas field (left). Right: Comparison between calculated p/z (red) to values determined by (2017).

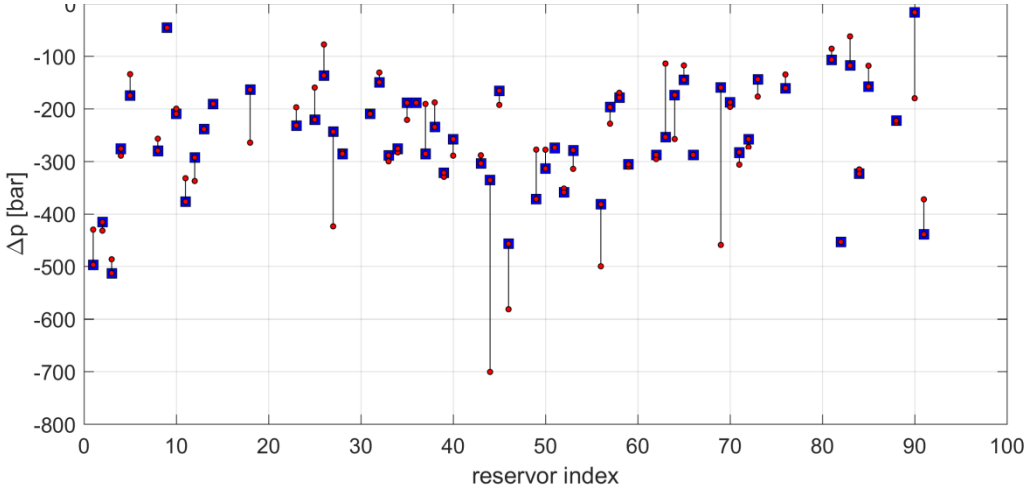

Figure 33: Comparison of calculated reservoir depletion (red dots) to the depletion values stated in the primary data sources (blue squares). Calculated depletion is based on $GIIP_{dyn}$ as provided by SodM (Table 9) and production data from nlog.nl.

APPENDIX B SIMULATION BENCHMARKS

Poroelastic models implemented in this study were benchmarked against numerical simulations performed by van den Bogert (2016). Simulation results of van den Bogert (2016) could almost exactly be reproduced by the numerical models implemented in this study (see examples in Figure 34 and Figure 35).

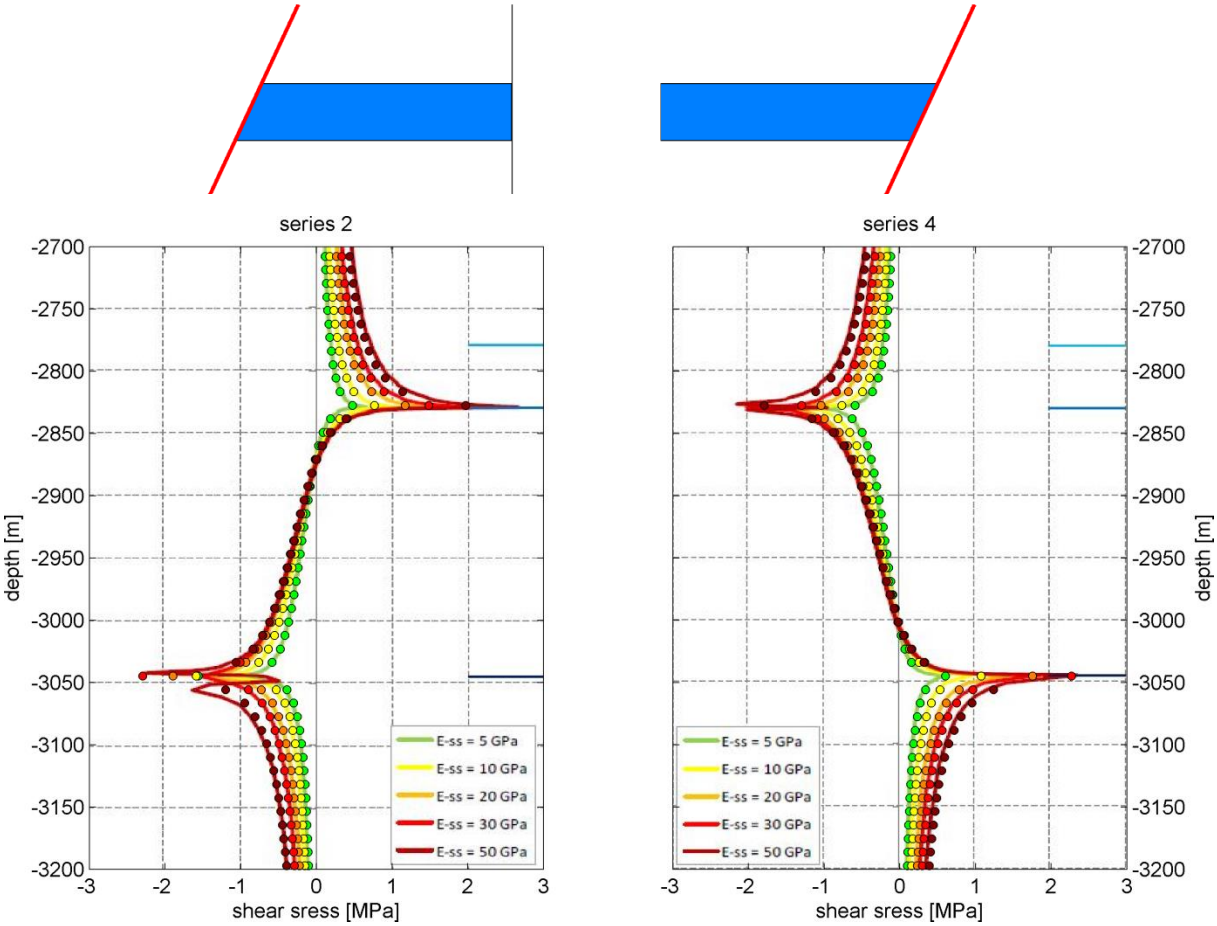

Figure 34: Comparison between simulation results of van den Bogert, 2016 (solid lines) to those of the current study (coloured dots). Results are in almost exact agreement. This is figure 4.9 in van den Bogert (2016), overlain with our simulation results. The underlying model is one-sided 2 MPa depletion with 65° fault dip (see schematic on top). Colour encoding denotes variations of Young's modulus.

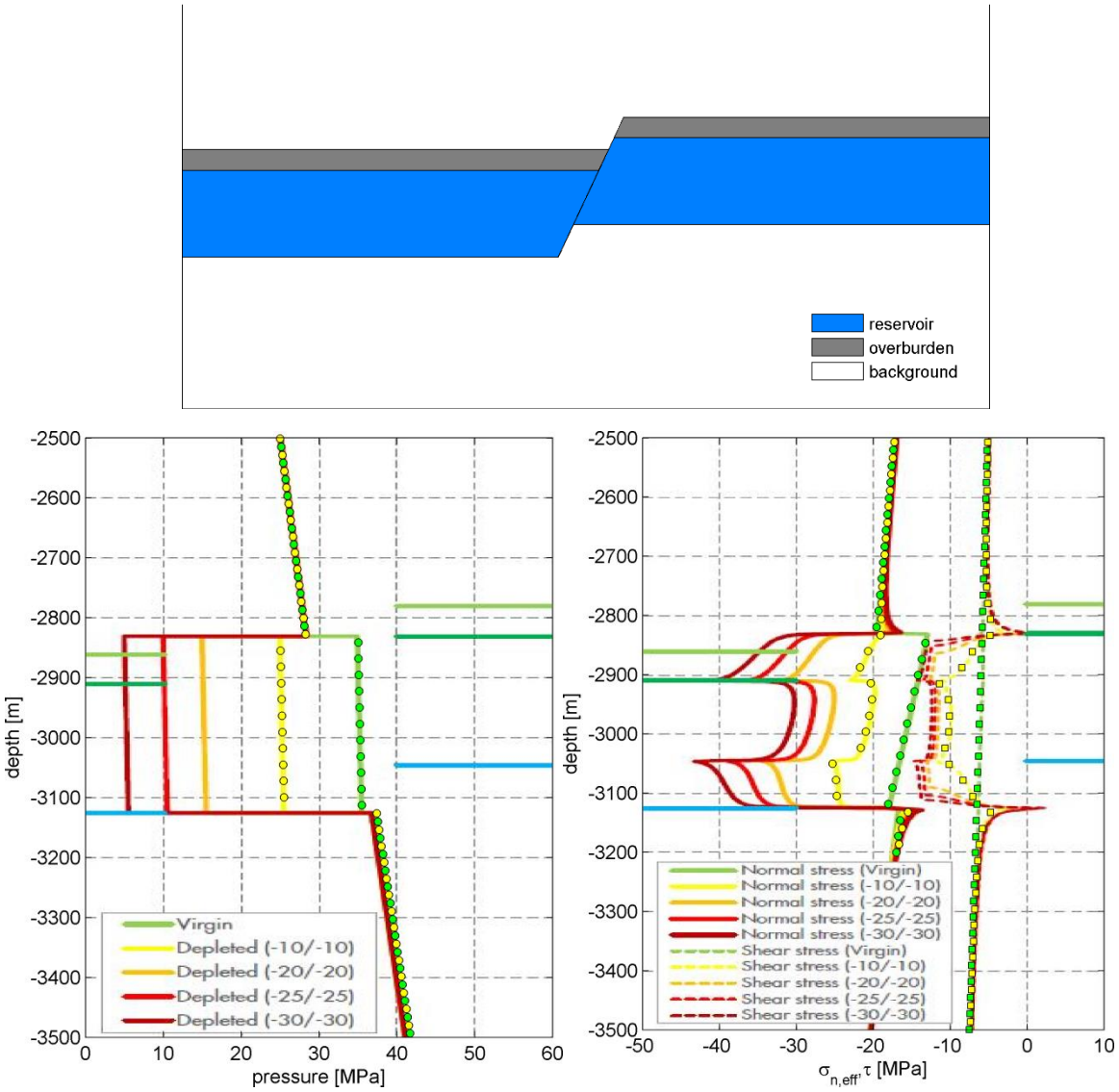

Figure 35: Comparison between simulation results of van den Bogert, 2016 (solid lines) to those of the current study (coloured dots). Results are in almost exact agreement. This is figure 7.1 in van den Bogert (2016), overlain with our simulation results. The underlying model is a two-sided depletion with 65° fault dip (see schematic on top). Colour encoding denotes variations of the depletion level and different stress components.

APPENDIX C

C.1. Best fit models

List of unconstrained parameter combinations resulting in a match of all category A reservoirs and 10 matches for category D reservoirs.

index	throw [m]	dip	k_{Sh}	k_{SH}	trend S_H	μ	C_0 [MPa]
BFM-P	100	70°	0.3	0.85	120°	0.8	1.93
1	100	65°	0.3	0.85	120°	0.8	1.95
2	150	70°	0.3	0.85	120°	0.8	1.96
3	150	65°	0.3	0.85	120°	0.8	1.99

Table 11: List of unconstrained parameter combinations in the best fitting models.

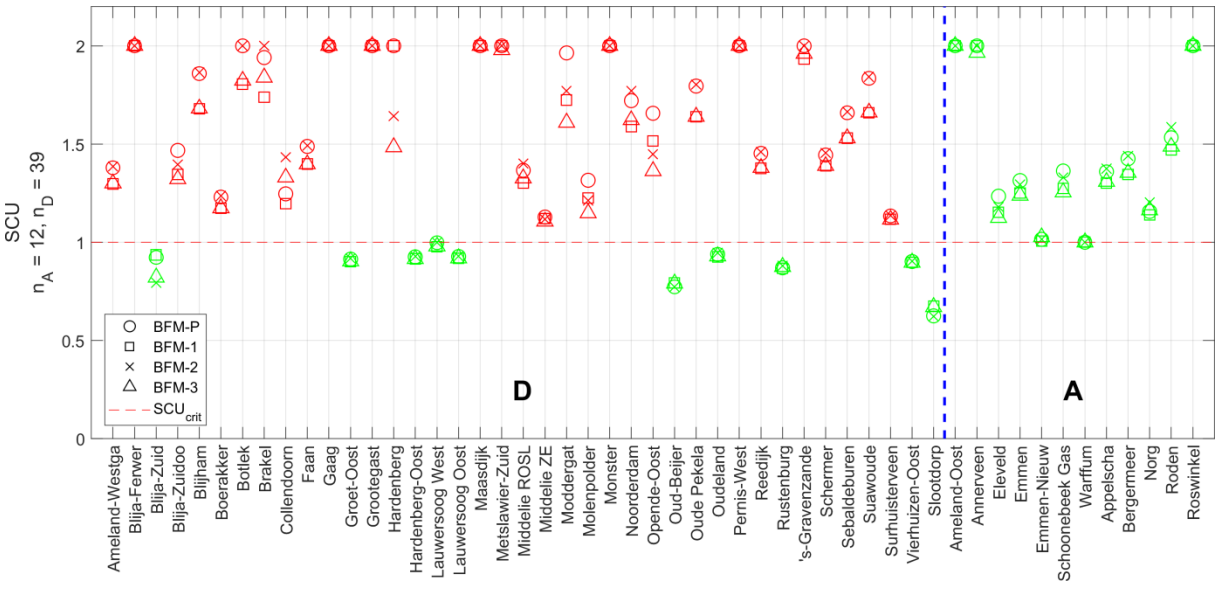

Figure 36: Comparison of SCU-values for the best-fit models in Table 11 (model index according to legend). Although unconstrained parameter vary between the models, it is always the same reservoirs for which simulation results are in accordance with observations. Green colours denote simulation results matching observations, red colours those not in accordance with observations. SCU values saturated at a level of 2 for displaying purposes.

Appendix C

reservoir	SCU			
	BFM-P	1	2	3
's-Gravenzande	2.19	1.93	2.24	1.96
Ameland-Oost	7.25	4.50	2.82	2.30
Ameland-Westgat	1.38	1.30	1.39	1.30
Anjum	1.55	1.43	1.56	1.43
Annerveen	3.41	2.67	2.28	1.97
Appelscha	1.36	1.30	1.37	1.31
Bedum	1.19	1.16	1.19	1.16
Bergen ROSL	1.08	1.04	1.09	1.05
Bergermeer	1.43	1.35	1.44	1.35
Blija-Ferwerderadeel	4.91	3.38	3.92	2.92
Blija-Zuid	0.92	0.94	0.79	0.82
Blija-Zuidoost	1.47	1.34	1.40	1.32
Blijham	1.86	1.68	1.86	1.68
Boerakker	1.23	1.17	1.24	1.17
Botlek	2.01	1.81	2.05	1.82
Brakel	1.94	1.74	2.09	1.84
Coevorden ZE	1.52	1.42	1.51	1.41
Collendoorn	1.25	1.20	1.43	1.33
Dalen ZE	1.47	1.38	1.46	1.37
Den Velde DC	0.68	0.70	0.68	0.70
Den Velde ZE	1.22	1.13	1.16	1.10
Eleveld	1.23	1.15	1.18	1.12
Eleveld NN	0.36	0.37	0.41	0.42
Emmen	1.31	1.25	1.29	1.24
Emmen-Nieuw Amsterdam	1.01	1.01	1.01	1.03
Faan	1.49	1.40	1.49	1.40
Gaag	6.70	4.09	7.51	4.38

reservoir	SCU			
	BFM-P	1	2	3
Groet	1.74	1.58	1.75	1.59
Groet-Oost	0.91	0.90	0.92	0.90
Grootegast	5.03	3.45	5.04	3.48
Hardenberg	2.47	2.08	1.64	1.49
Hardenberg-Oost	0.93	0.92	0.93	0.91
Kiel-Windeweer	2.06	1.81	1.19	1.13
Kollum	1.08	1.03	0.98	0.95
Kollum-Noord	1.58	1.42	1.24	1.17
Kommerzijl	1.54	1.44	1.65	1.51
Lauwersoog Oost	0.93	0.92	0.93	0.92
Lauwersoog West	1.00	0.98	1.00	0.98
Leens	1.55	1.44	1.55	1.44
Maasdijk	2.61	2.19	3.01	2.45
Marum	1.46	1.36	1.29	1.24
Metslawier	4.70	3.42	2.25	1.93
Metslawier-Zuid	3.86	2.95	2.31	1.98
Middelie ROSL	1.37	1.30	1.40	1.33
Middelie ZE	1.13	1.12	1.12	1.11
Moddergat	1.96	1.72	1.77	1.61
Molenpolder	1.32	1.22	1.21	1.15
Monster	6.20	3.96	2.94	2.38
Munnekezijl	2.27	1.96	1.29	1.21
Noorderdam	1.72	1.59	1.77	1.62
Norg	1.16	1.14	1.20	1.16
Oosterhesselen DC	0.63	0.65	0.63	0.65
Oosterhesselen ZE	2.02	1.79	2.03	1.80
Oostrum	1.24	1.18	1.24	1.18

reservoir	SCU			
	BFM-P	1	2	3
Opende-Oost	1.66	1.52	1.45	1.36
Oud-Beijerland Zuid	0.77	0.79	0.77	0.79
Oude Pekela	1.80	1.64	1.80	1.64
Oudeland	0.94	0.93	0.95	0.93
Pasop	3.92	2.93	3.35	2.63
Pernis-West	5.81	3.76	6.34	3.98
Reedijk	1.45	1.38	1.46	1.38
Roden	1.53	1.47	1.59	1.49
Roswinkel	3.70	2.84	2.76	2.26
Rustenburg	0.87	0.87	0.88	0.87
Saaksum Oost	1.32	1.26	1.32	1.26
Saaksum West	0.96	0.95	0.96	0.95
Schermer	1.44	1.39	1.46	1.39
Schoonebeek Gas	1.36	1.27	1.33	1.26
Sebaldeburen	1.66	1.53	1.66	1.53
Slootdorp	0.63	0.68	0.62	0.67
Suawoude	1.83	1.66	1.84	1.66
Surhuisterveen	1.13	1.12	1.14	1.12
Tietjerksteradeel ROSL	5.55	3.68	2.21	1.90
Ureterp	1.41	1.32	1.28	1.23
Vierhuizen-Oost	0.90	0.90	0.90	0.90
Vries Centraal	1.82	1.65	1.44	1.34
Vries Noord	0.93	0.94	1.01	1.01
Vries Zuid	2.43	2.07	1.73	1.57
Warffum	1.00	1.00	1.00	1.00
Witterdiep	1.08	1.08	1.12	1.10
Zuidwending-Oost	1.89	1.71	1.90	1.71

Table 12: SCU-values for the best-fit models in Table 11.

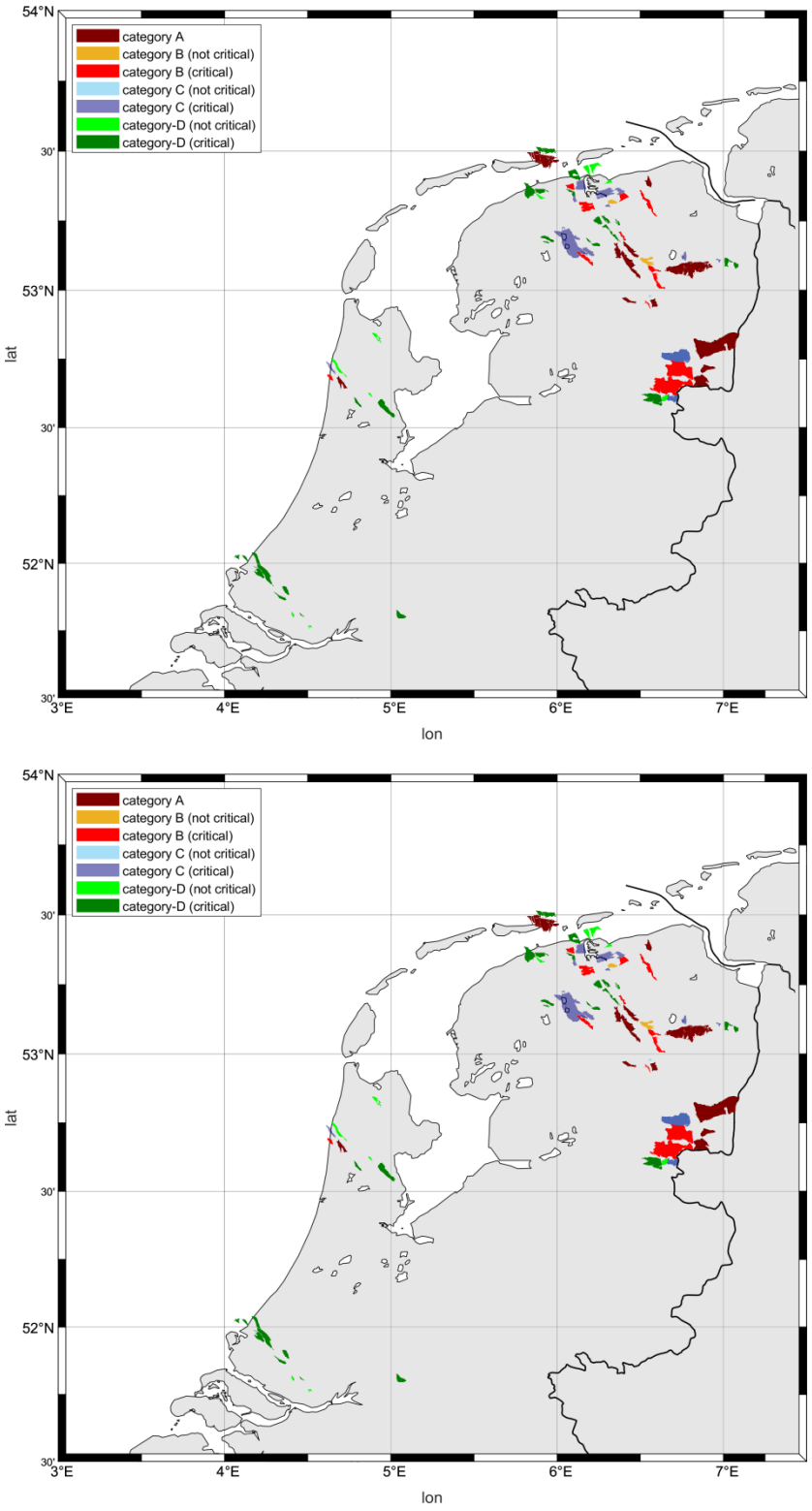

Figure 37: Simulation results for best fit models BFM-P (top) & BFM-1 (bottom) according to Table 11 and colour-scaled with respect to reservoir category.

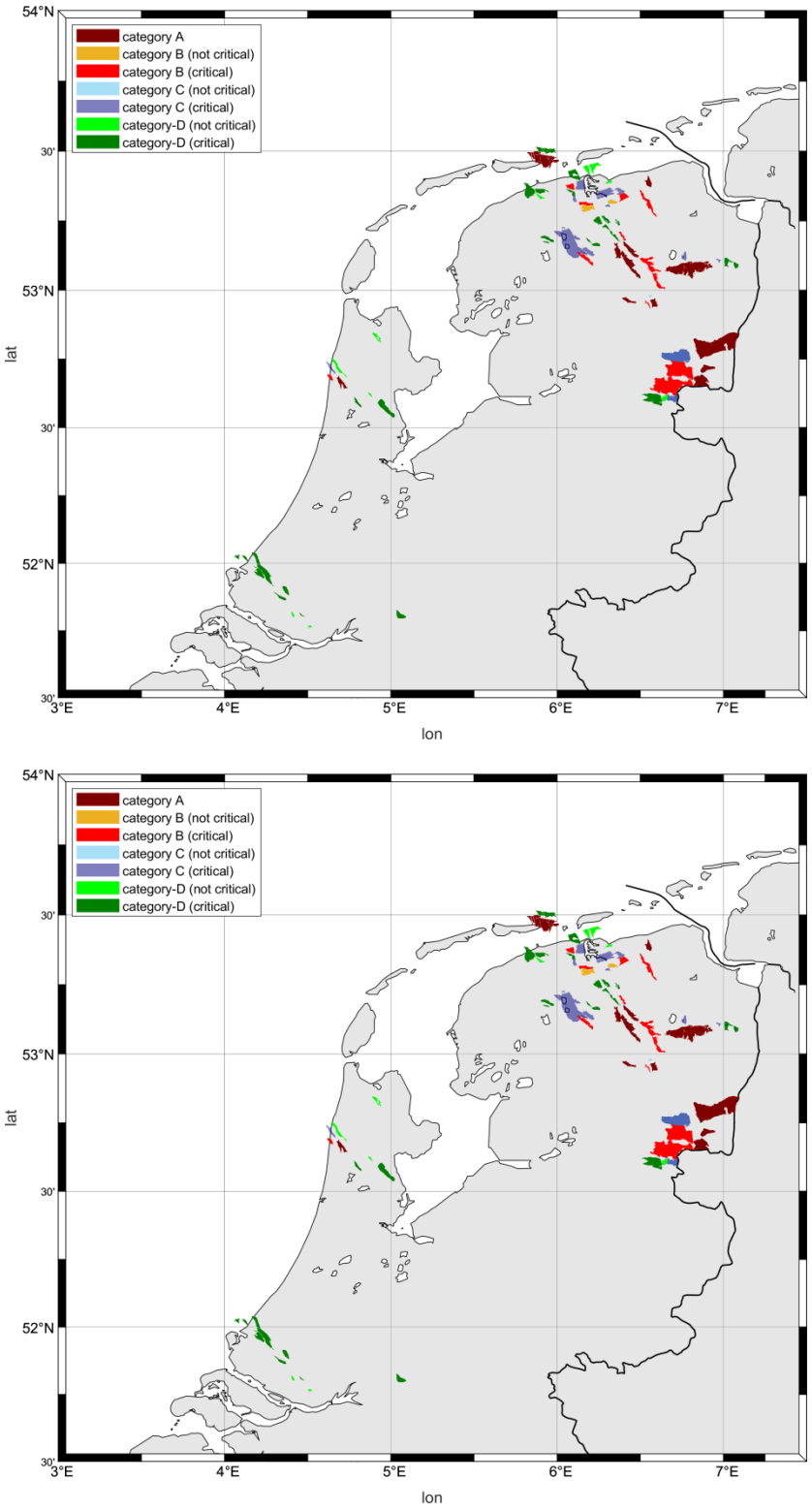

Figure 38: Simulation results for best fit models BFM-3 (top) & BFM-4 (bottom) according to Table 11 and colour-scaled with respect to reservoir category.

C.2. Critical patch length

In the current study, SCU is smoothed along the fault on 10 m segments to reduce the effect of stress peaks that occur at layer boundaries in the numerical model (compare section 4.2.2).

To investigate the sensitivity of our study results to the assumed smoothing length of 10 m, we have performed additional simulations using a smoothing length of 35 m. All simulations are based on BFM-P model parameters.

Figure 39 compares the resulting SCU values. As could be expected, an overall shift of criticality towards lower values with increasing patch length is observed. By this, 2 category A reservoirs become sub-critical in the BFM-P model (mismatch). Since all reservoirs are shifted towards smaller SCU values, however, global parameters could be adjusted such the overall criticality level implicitly determined by these parameters is increased (e.g. by lowering C_0). Although we have not repeated the calibration procedure (section 4.3) using 35 m smoothing length, it can be expected from Figure 39 that an equivalent set of global model parameters can be found resulting in exactly the same matches of category A and category D reservoirs.

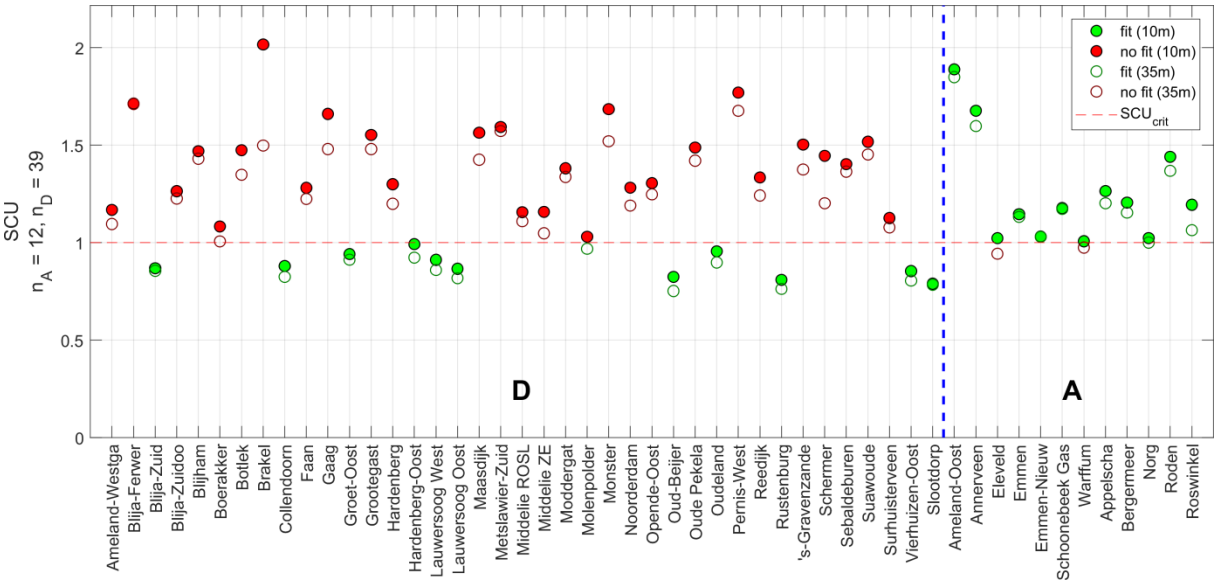

Figure 39: Comparison of SCU values simulated with 10 m smoothing (solid circles) and 35 m smoothing (open circles) length, respectively. All simulations are based on BFM-P model parameters. Dashed blue line separates category D reservoirs from category A reservoirs.

C.3. Results for category B and C reservoirs

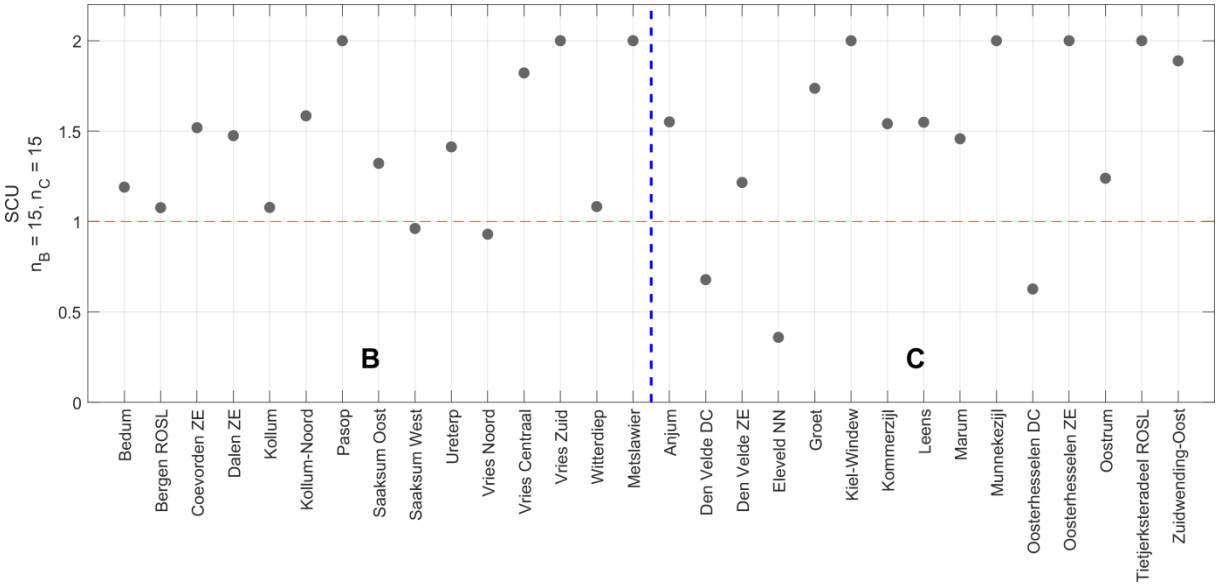

Figure 40: Numerically simulated SCU values based on the BFM-P and BFM-SW model for category B and category C reservoirs. Dashed blue line separates category B from category C reservoirs, dashed red line outlines crititical SCU-value. Note that the difference between BFM-P and BFM-SW is restricted to reservoirs in the South-West that are all category D reservoirs.

C.4. SCU values BFM-SW

reservoir	SCU	category
's-Gravenzande	0,61	D
Ameland-Oost	7,25	A
Ameland-Westgat	1,38	D
Anjum	1,55	C
Annerveen	3,41	A
Appelscha	1,36	A
Bedum	1,19	B
Bergen ROSL	1,08	B
Bergermeer	1,43	A
Blija-Ferwerderadeel	4,91	D
Blija-Zuid	0,92	D
Blija-Zuidoost	1,47	D
Blijham	1,86	D
Boerakker	1,23	D
Botlek	0,58	D
Brakel	0,68	D
Coevorden ZE	1,52	B
Collendoorn	1,25	D
Dalen ZE	1,47	B
Den Velde DC	0,68	C
Den Velde ZE	1,22	C
Eleveld	1,23	A
Eleveld NN	0,36	C
Emmen	1,31	A
Emmen-Nieuw Amsterdam	1,01	A
Faan	1,49	D
Gaag	0,9	D

reservoir	SCU	category
Groet	1,74	C
Groet-Oost	0,91	D
Grootegast	5,03	D
Hardenberg	2,47	D
Hardenberg-Oost	0,93	D
Kiel-Windeweer	2,06	C
Kollum	1,08	B
Kollum-Noord	1,58	B
Kommerzijl	1,54	C
Lauwersoog Oost	0,93	D
Lauwersoog West	1	D
Leens	1,55	C
Maasdijk	0,84	D
Marum	1,46	C
Metslawier	4,7	B
Metslawier-Zuid	3,86	D
Middelie ROSL	1,37	D
Middelie ZE	1,13	D
Moddergat	1,96	D
Molenpolder	1,32	D
Monster	0,95	D
Munnekezijl	2,27	C
Noorderdam	0,46	D
Norg	1,16	A
Oosterhesselen DC	0,63	C
Oosterhesselen ZE	2,02	C
Oostrum	1,24	C

reservoir	SCU	category
Opende-Oost	1,66	D
Oud-Beijerland Zuid	0,29	D
Oude Pekela	1,8	D
Oudeland	0,4	D
Pasop	3,92	B
Pernis-West	0,86	D
Reedijk	0,4	D
Roden	1,53	A
Roswinkel	3,7	A
Rustenburg	0,87	D
Saaksum Oost	1,32	B
Saaksum West	0,96	B
Schermer	1,44	D
Schoonebeek Gas	1,36	A
Sebaldeburen	1,66	D
Slootdorp	0,63	D
Suawoude	1,83	D
Surhuisterveen	1,13	D
Tietjerksteradeel ROSL	5,55	C
Ureterp	1,41	B
Vierhuizen-Oost	0,9	D
Vries Centraal	1,82	B
Vries Noord	0,93	B
Vries Zuid	2,43	B
Warffum	1	A
Witterdiep	1,08	B
Zuidwending-Oost	1,89	C

Table 13: List of SCU-values for the BFM-SW model.